In-plane failure surfaces for masonry with joints of finite thickness estimated by a Method of Cells-type approach

Gabriele Milani [a,*], Alberto Taliercio [b]

[a] Department of Architecture, Built Environment & Construction Engineering, Politecnico di Milano, Piazza Leonardo da Vinci 32, 20133 Milan, Italy
[b] Department of Civil and Environmental Engineering, Politecnico di Milano, Piazza Leonardo da Vinci 32, 20133 Milan, Italy

Received 28 June 2014
Accepted 8 December 2014
Available online 10 January 2015

1. Introduction

In the last decades, there has been a growing interest in the mathematical description of the mechanical behavior of brick masonry beyond the elastic limit and up to collapse. A number of theoretical [1,2] and experimental studies [3] have been carried out, with the aim of providing reliable and efficient tools for the safety assessment of masonry structures, including monuments and buildings of historical value.

Micro-modelling is, in principle, the most refined approach to analyze masonry structures [4–8], and heterogeneous bodies in general, as the geometry and the mechanical properties of the constituent materials can be explicitly taken into account with any degree of accuracy. An intrinsic drawback of this approach is the need of modelling units and mortar joints separately. Although most authors assume joints to be interfaces of vanishing thickness, the computational effort of any micro-modelling approach is proportional to the number of bricks the structure consists of, so that its applicability is limited to small panels.

At the other extreme is macro-modelling [9–15], which does not make any distinction between units and joints, and aims at defining the mechanical properties of an equivalent homogeneous material.

Homogenization [16–24] is a fair compromise between micro- and macro-modelling. Indeed, the mechanical properties of the macroscopically equivalent material are derived from those of the constituents (brick and mortar), which can be easily obtained through cheap tests on small specimens. Once these properties have been estimated through the analysis of a Representative Volume Element (RVE), fairly rough finite element meshes can be employed to analyze large masonry buildings, assumed to consist of a homogeneous (anisotropic) material.

The major drawback of homogenization in non-linear FE computations is that a continuous interaction between meso- and macro-scale is needed. This dramatically increases the computational effort, as the field equations have to be numerically solved at each loading step, at all the integration points. For the above reasons, limit analysis combined with homogenization theory seems to be one of the most powerful and straightforward structural analysis tools to predict the ultimate bearing capacity of masonry structures in a fast and reliable way.

Different homogenization models have been recently proposed in the technical literature for the evaluation of homogenized strength domains for in-plane [20–23] and out-of-plane loaded [24–30] masonry walls. Assuming both units and joints to consist of rigid plastic materials with associated flow rule, the classical

* Corresponding author. Tel.: +39 022399 4290; fax: +39 022399 4220.
E-mail address: gabriele.milani@polimi.it (G. Milani).

upper and lower bound theorems of limit analysis can be applied to any RVE to approximate the macroscopic strength domain of masonry. In particular, according to the lower bound theorem, any divergence-free plastically admissible micro-stress field, such that the stress vector is anti-periodic over the boundary of the RVE, allows a lower bound to the actual homogenized failure domain to be obtained by means of a constrained maximization problem. Conversely, the upper bound theorem deals with kine-matically admissible velocity fields fulfilling suitable periodicity conditions, and allows upper bounds to the actual homogenized failure domain to be obtained by means of the constrained minimi-zation of the internal dissipated power. In both cases, the mechan-ical problem is translated into a mathematical (non-)linear programming problem, with a reduced number of variables.

In the present work, the upper bound theorem of limit analysis is employed to estimate the macroscopic strength domain of in-plane loaded masonry walls, taking the finite thickness of the joints and the limited strength of both components into account. The advantage of this approach compared to existing proposals is the accuracy in the definition of the macroscopic domain, combined with the simplicity of the proposed velocity field, which depends on a very limited number of parameters.

The layout of the paper is as follows. In Section 2, the kinematic definition of the macroscopic strength domain of periodic hetero-geneous media [31] is briefly recalled. The original model is pre-sented in Section 3. In Section 3.1 a simple periodic velocity field is proposed, dividing any RVE into sub-cells according to the so-called Method of Cells (MoC) [32,33]. The ensuing limit analysis problem formulated over the RVE is detailed in Section 3.2. The main advantages of the proposed approach are summarized in Sec-tion 3.3. The model is applied in Section 4 to estimate the uniaxial off-axis compressive strength of wallettes, for which closed-form expressions are available in the literature [34,35]. In Section 5 a few models available in the literature to predict the macroscopic strength of masonry are briefly reviewed [22,26,27]: the biaxial strength domains given by the MoC at any orientation of the prin-cipal stresses to the joints are compared with those predicted by the existing models in Section 6. The failure surfaces predicted by the MoC are compared in Section 7 with the experimental results of biaxial compression tests carried out by other authors [36] on masonry panels. The implementation of the proposed crite-rion in a finite element code is illustrated in Section 8: the code is applied in Section 9 to predict the limit load of a deep beam. Com-parisons with the predictions given by refined heterogeneous mod-els, which accurately take the masonry texture into account, are also reported, to emphasize the accuracy of the proposed approach for any joint thickness. Finally, in Section 10 the main findings of the work are summarized and future perspectives of the research are outlined.

2. Homogenization for rigid-plastic periodic media: Kinematic definition of the macroscopic strength domain

Masonry is a composite material usually made of units bonded with mortar joints. In most cases of building practice, units and mortar are periodically arranged. Owing to periodicity, any wall Ω can be seen as the repetition of a Representative Volume Element Y (RVE, or unit cell). Y contains all the information necessary to completely describe the macroscopic behavior of Ω. If a running bond or a header bond pattern is considered (Fig. 1a), it is expedient to choose an elementary cell of rectangular shape (Fig. 1b).

To define the macroscopic (or global, or average) mechanical properties of masonry, homogenization techniques can be used both in the elastic and inelastic range, taking into account the micro-structure only at a cell level. This leads to a significant sim-plification of the numerical models adopted to analyze entire masonry buildings, especially in the inelastic field.

The basic idea of any homogenization procedure consists in defining averaged quantities representing the macroscopic stress $\boldsymbol{\Sigma}$ and the macroscopic strain rate $\boldsymbol{D}$ as follows:

$$\boldsymbol{\Sigma} = \frac{1}{A}\int_Y \boldsymbol{\sigma}(\boldsymbol{y})dY, \quad \boldsymbol{D} = \frac{1}{A}\int_{\partial Y} \boldsymbol{v}(\boldsymbol{y}) \overset{s}{\otimes} \boldsymbol{n}(\boldsymbol{y})dS \tag{1}$$

where A is the area of the RVE, $\boldsymbol{y}$ is any point in Y or on its boundary ∂Y, $\boldsymbol{\sigma}$ is the microscopic (local) stress field, $\boldsymbol{v}$ is the local velocity field, $\boldsymbol{n}$ is the unit outward normal vector to ∂Y, and $\overset{s}{\otimes}$ denotes the symmetric part of the dyadic product $\boldsymbol{v} \otimes \boldsymbol{n}$. Eq. (1) applies in general to microscopic non-differentiable velocity fields.

$\boldsymbol{\sigma}$ and $\boldsymbol{v}$ must fulfil suitable periodicity conditions to match the periodicity of the heterogeneous medium:

$$\begin{cases} \boldsymbol{v} = \boldsymbol{D}\boldsymbol{y} + \tilde{\mathbf{v}}, & \tilde{\mathbf{v}} \text{ periodic on } Y \quad \text{(a)} \\ \boldsymbol{\sigma}\boldsymbol{n} & \text{anti} - \text{periodic on } \partial Y \quad \text{(b)} \end{cases} \tag{2}$$

Any velocity field fulfilling Eq. (2a) is said to be "strain-rate periodic".

The kinematic definition of the homogenized strength domain of masonry, say S^{hom}, is due to Suquet [31] and makes use of the definition of the support function of this domain, $\pi^{\text{hom}}(\boldsymbol{D})$, which reads:

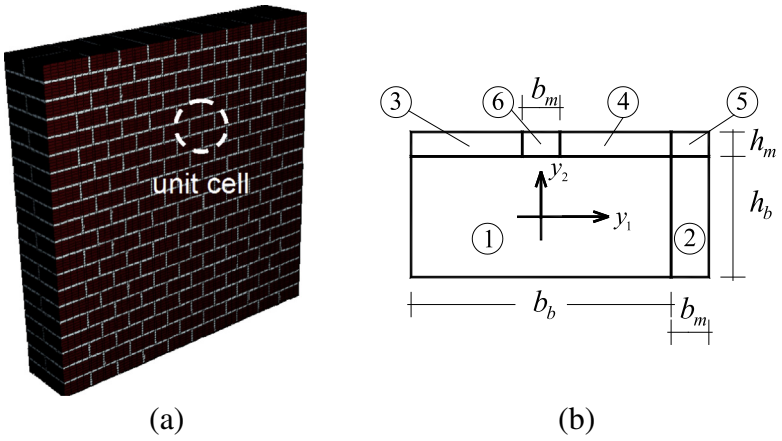

Fig. 1. (a) Running or header bond brick wall; (b) rectangular RVE and subdivision into sub-cells.

$$S^{\hom}=\left\{\boldsymbol{\Sigma}\left|\begin{array}{c}\boldsymbol{\Sigma}:\boldsymbol{D}\leqslant\pi^{\hom}(\boldsymbol{D})\quad\forall\boldsymbol{D}\in R^6\\ \pi^{\hom}(\boldsymbol{D})=\inf_{\boldsymbol{v}}\left\{P(\boldsymbol{v})|\boldsymbol{D}=\frac{1}{A}\int_{\partial Y}\boldsymbol{v}\overset{s}{\otimes}\boldsymbol{n}dS\right\}\\ P(\boldsymbol{v})=\int_Y\pi(\boldsymbol{d})dY+\int_{S_v}\pi([[\boldsymbol{v}]];\boldsymbol{n}_v)dS\end{array}\right.\right\}\tag{3}$$

where

- $\pi(\boldsymbol{d})=\sup_{\boldsymbol{\sigma}}\{\boldsymbol{\sigma}:\boldsymbol{d};\boldsymbol{\sigma}\in S(\boldsymbol{y})\}$ is the support function of the strength domain at $\boldsymbol{y}$;
- S_v is any discontinuity surface for $\boldsymbol{v}$ in Y, and $\boldsymbol{n}_v$ is the normal to S_v;
- $[[\boldsymbol{v}]]$ is the jump in velocity across S_v;
- $\pi([[\boldsymbol{v}]];\boldsymbol{n}_v)=\pi\left([[\boldsymbol{v}]]\overset{s}{\otimes}\boldsymbol{n}_v\right)$.

Using Eq. (3), de Buhan and De Felice explicitly determined the homogenized strength domain of masonry in the space of the macroscopic stresses, assuming units to be infinitely resistant and joints to be interfaces of vanishing thickness obeying the Mohr–Coulomb strength criterion [20]. If no approximation is made regarding the strength and the geometry of the components, Eq. (3) allows upper bounds to the macroscopic strength domain to be obtained by defining failure mechanisms fulfilling suitable periodicity conditions over the RVE.

From here onwards, units will be supposed to be perfectly bonded to mortar joints, so that no jump in displacements occurs within the RVE. Note, however, that Eq. (3) allows discontinuous microscopic velocity fields to be taken into account.

3. The proposed method: Formulation and motivations

The motivation to propose a new homogenization model in the rigid-plastic case is twofold. Firstly, the models available in the literature do not take the actual thickness of the joints into account and neglect the possibility of brick failure, which occurs under several stress combinations. Secondly, it is of paramount importance for the effective safety assessment of large masonry buildings to have simple models available, which do not require any refined discretization of the elementary cell to estimate the macroscopic masonry strength, thus avoiding time-consuming elasto-plastic incremental FE analyses. Another advantage of approaches needing few variables to describe the macroscopic response of masonry is that they can easily accommodate the strainsoftening and crushing behavior of the constituents if elasto-damaging material models are taken into account to match experimental evidences more closely.

Here, an approach based on the so-called Method of Cells (MoC) is proposed. The MoC was originally formulated by Abo-udi [32] for unidirectional composites reinforced by a regular pattern of long, reinforcing fibers, and has been recently extended by Taliercio [33] to determine the macroscopic elastic and creep coefficients of masonry in closed form. The method, applied to in-plane loaded running or header bond masonry, consists in the subdivision of the RVE into rectangular sub-cells, as shown in Fig. 1b, where the velocity field is approximated using two sets of strain-rate periodic piecewise differentiable velocity fields: one describing the deformation mode under normal stresses; the other, describing a shear-type deformation mode.

3.1. Kinematic assumptions

Let $v_1^{n(i)}$ and $v_2^{n(i)}$ denote the horizontal and vertical velocity components in the ith sub-cell when the RVE undergoes normal stresses parallel to the bed and the head joints. These components are given the same expressions proposed by Taliercio [33] in terms of displacements in the elastic range, which read:

$$\begin{aligned}
&v_1^{n(2)}=2U_1\frac{y_1}{b_b},\quad v_2^{n(1)}=-2W_1\frac{y_2}{h_b}\\
&v_1^{n(2)}=U_1+\frac{(U_2-U_1)\left(y_1-\frac{b_b}{2}\right)}{b_m},\quad v_2^{n(2)}=v_2^{n(1)}\\
&v_1^{n(3)}=v_1^{n(1)}-\frac{(U_1(1+2\alpha_b)-U_2)\left(\frac{h_b}{2}-y_2\right)}{2h_m},\quad v_2^{n(3)}=-W_1+\frac{(W_1-W_2)\left(y_2-\frac{h_b}{2}\right)}{h_m}\\
&v_1^{n(4)}=v_1^{n(1)}+\frac{(U_1(1+2\alpha_b)-U_2)\left(\frac{h_b}{2}-y_2\right)}{2h_m},\quad v_2^{n(4)}=v_2^{n(3)}\\
&v_1^{n(5)}=U_1-\frac{(U_1(1+2\alpha_b)-U_2)\left(\frac{b_b+b_m}{2}-y_1\right)\left(y_2-\frac{h_b}{2}\right)}{b_mh_m}-\frac{(U_1-U_2)\left(y_1-\frac{b_b}{2}\right)}{b_m},\quad v_2^{n(5)}=v_2^{n(3)}\\
&v_1^{n(6)}=2\frac{y_1}{b_b}\left(U_1-\frac{\left(U_1+\frac{U_1-U_2}{2\alpha_b}\right)\left(y_2-\frac{h_b}{2}\right)}{h_m}\right),\quad v_2^{n(6)}=v_2^{n(3)}
\end{aligned}\tag{4}$$

where b_b is the brick length, h_b is the brick height, b_m is the thickness of the head joints, h_m is the thickness of the bed joints, and $\alpha_b=b_m/b_b$ (see Fig. 1b). The origin of the local reference frame Oy_1y_2 is located at the center of sub-cell 1 (brick).

The velocity field (4) is fully defined by four 'degrees of freedom' (DOFs), U_1, U_2, W_1 and W_2 (see Fig. 2).

When a shear deformation mode is applied on the RVE, the following velocity fields are assumed within each sub-cell:

$$\begin{aligned}
&v_1^{t(1)}=2U_1^t\frac{y_2}{h_b},\quad v_2^{t(1)}=0,\quad v_1^{t(2)}=v_1^{t(1)},\quad v_2^{t(2)}=W_1^t\frac{y_1-\frac{b_b}{2}}{b_m}\\
&v_1^{t(3)}=U_1^t+\frac{U_2^t-U_1^t}{h_m}\left(y_2-\frac{h_b}{2}\right),\quad v_2^{t(3)}=-W_2^t\frac{y_2-\frac{h_b}{2}}{h_m}\\
&v_1^{t(4)}=v_1^{t(3)},\quad v_2^{t(4)}=-v_2^{t(3)}\\
&v_1^{t(5)}=v_1^{t(3)},\quad v_2^{t(5)}=-W_1^t\frac{\left(y_1-\frac{b_b+b_m}{2}\right)\left(y_2-\frac{h_b}{2}\right)-h_m\left(y_1-\frac{b_b}{2}\right)}{b_mh_m}\\
&v_1^{t(6)}=v_1^{t(3)},\quad v_2^{t(6)}=W_1^t\frac{y_1\left(y_2-\frac{h_b}{2}\right)}{b_mh_m}
\end{aligned}\tag{5}$$

with $W_1^t=2W_2^t$. The symbols $v_1^{t(i)}$ and $v_2^{t(i)}$ denote the horizontal and vertical velocity components in the ith sub-cell under macro-scopic shear stress. This velocity field is completely defined by three DOFs, namely U_1^t, U_2^t and W_1^t. Their physical meaning is depicted in Fig. 3.

Within each sub-cell, the velocity field defined by Eqs. (4) and (5) is either linear (sub-cells 1, 2, 3, 4) or bilinear (sub-cells 5, 6) under any macroscopic stress condition. Accordingly, plastic strains vary at most linearly within each sub-cell. This assumption is not supported by any empirical evidence: whereas it can be reasonable for thin mortar joints, it might become questionable as the joint thickness increases. Note, however, that a similar assumption made in the linear field led to excellent predictions of the

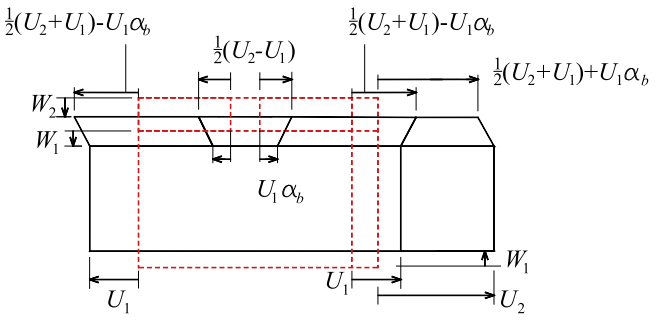

Fig. 2. Strain-periodic kinematically admissible velocity field under horizontal or vertical macroscopic normal stresses.

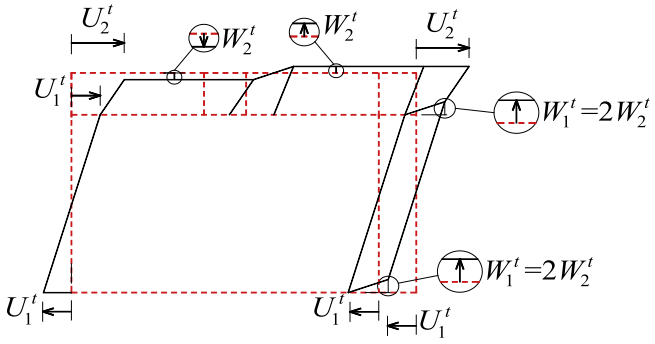

Fig. 3. Strain-periodic kinematically admissible velocity field under macroscopic shear stress.

macroscopic elastic and creep coefficients of brick masonry for any joint thickness [33].

Assuming that both mortar and bricks behave as rigid plastic materials obeying an associated flow rule, an outer bound to the homogenized strength domain of masonry can be obtained solving problem (3). For non-standard materials, the domain S^{hom} defined according to Eq. (3) is itself only an outer bound to the real macroscopic strength domain (see e.g. [37]). In any case, a linear programming problem is obtained, where the objective function to be minimized is the total internal dissipated power π^{hom}.

3.2. The limit analysis problem at the cell level: Homogenized failure surfaces

According to the kinematic theorem of limit analysis, and assuming the velocity field over the RVE to be approximated by means of the expressions provided by Eqs. (4) and (5), the associativity of the plastic flow over each sub-cell must be prescribed.

Let $v_1 = v_1^{n(i)} + v_1^{t(i)}$ and $v_2 = v_2^{n(i)} + v_2^{t(i)}$ denote the horizontal and vertical components of the velocity field in the (i)th sub-cell. At each point of any sub-cell, the associated flow rule translates into three equality constrains, which can be written as $\dot{\boldsymbol{\varepsilon}}_{pl}^{(i)} = \left[\frac{\partial v_1}{\partial y_1} \quad \frac{\partial v_2}{\partial y_2} \quad \frac{\partial v_1}{\partial y_2} + \frac{\partial v_2}{\partial y_1}\right] = \dot{\lambda}^{(i)} \frac{\partial S^{b,m}}{\partial \boldsymbol{\sigma}}$, where $\dot{\boldsymbol{\varepsilon}}_{pl}^{(i)}$ is the plastic strain rate field in the (i)th sub-cell, $\dot{\lambda}^{(i)}$ ($\geqslant 0$) is the rate of the plastic multiplier, and $S^{b,m}$ is the (non) linear failure surface of either bricks (b) or mortar (m). Let the failure surfaces of bricks and mortar be approximated by m planes, so that each strength criterion is defined by a set of linear inequalities of the form $S^{b,m} \equiv \mathbf{A}^{in}\boldsymbol{\sigma} \leqslant \mathbf{b}^{in}$. As $\dot{\boldsymbol{\varepsilon}}_{pl}^{(i)}$ varies at most linearly within each sub-cell, plastic admissibility is checked only at three of the corners. Hence, nine linear equality constraints per sub-cell are introduced in matrix form as $\mathbf{A}_{U(i)}^{eq}\mathbf{U} + \mathbf{A}_{\lambda(i)}^{eq}\dot{\boldsymbol{\lambda}}^{(i)} = \mathbf{0}$, where $\mathbf{U}$ is an array collecting the 7 DOFs describing the microscopic velocity field (i.e. $\mathbf{U} = \{U_1, U_2, W_1, W_2, U_1^t, U_2^t W_1^t\}^T$, $\dot{\boldsymbol{\lambda}}^{(i)} = \left[\dot{\boldsymbol{\lambda}}_A^{(i)T} \quad \dot{\boldsymbol{\lambda}}_B^{(i)T} \quad \dot{\boldsymbol{\lambda}}_C^{(i)T}\right]^T$ is an array of $3m$ entries, collecting the rates of the plastic multipliers $\dot{\boldsymbol{\lambda}}_J^{(i)}$ at three of the corners of the rectangular sub-cell ($J = A, B, C$), and $\boldsymbol{A}_{U(i)}^{eq}$, $\mathbf{A}_{\lambda(i)}^{eq}$ are a 9×7 and a $9 \times 3m$ matrix, respectively. The plastic admissibility conditions are then assembled cell by cell into the following global system of equality constraints:

$$\mathbf{A}_U^{eq}\mathbf{U} + \mathbf{A}_\lambda^{eq}\dot{\boldsymbol{\lambda}} = \mathbf{0} \tag{6}$$

where $\mathbf{A}_U^{eq} = [\mathbf{A}_{U(1)}^{eqT} \dots \mathbf{A}_{U(6)}^{eqT}]^T$, $\dot{\boldsymbol{\lambda}} = [\dot{\boldsymbol{\lambda}}^{(1)T} \dots \dot{\boldsymbol{\lambda}}^{(6)T}]^T$, and $\mathbf{A}_\lambda^{eq}$ is a block matrix of dimension $(6{\cdot}9) \times (6{\cdot}3m)$, which can be expressed as:

$$\mathbf{A}_\lambda^{eq} = \mathbf{A}_{\lambda(1)}^{eq} \oplus \mathbf{A}_{\lambda(2)}^{eq} \oplus \cdots \oplus \mathbf{A}_{\lambda(6)}^{eq} \tag{7}$$

where $\oplus$ denotes direct sum.

Let B and C be a couple of corners at the opposite ends of one of the diagonals of the (i)th rectangular sub-cell. The internal power dissipated within the sub-cell can be written as:

$$P_{in}^{(i)} = \frac{\Omega^{(i)}}{2}\left(\mathbf{b}_{in}^{(i)T}\dot{\boldsymbol{\lambda}}_B^{(i)} + \mathbf{b}_{in}^{(i)T}\dot{\boldsymbol{\lambda}}_C^{(i)}\right) = \frac{\Omega^{(i)}}{2}\left[\mathbf{0}_{1\times m} \quad \mathbf{b}_{in}^{(i)T} \quad \mathbf{b}_{in}^{(i)T}\right]\dot{\boldsymbol{\lambda}}^{(i)} \tag{8}$$

where $\mathbf{0}_{1\times m}$ is an array of m zero entries and $\Omega^{(i)}$ is the area of the (i)th sub-cell. The power dissipated inside the whole RVE is obviously the sum of the contributions of each sub-cell, i.e.:

$$P_{in} = \sum_{i=1}^{6} \frac{\Omega^{(i)}}{2}\left[\mathbf{0}_{1\times m} \quad \mathbf{b}_{in}^{(i)T} \quad \mathbf{b}_{in}^{(i)T}\right]\dot{\boldsymbol{\lambda}}^{(i)} \tag{9}$$

Assume the 'external load' applied to the RVE (i.e., the macroscopic stress) to be a point of the homogenized failure surface. The array of the macroscopic stress components can be expressed as $\boldsymbol{\Sigma} = \Lambda[\alpha \quad \beta \quad \gamma]^T$, where Λ is the load multiplier and α, β, γ are director cosines defining the direction of $\boldsymbol{\Sigma}$ in the space of the homogenized in-plane stresses. Accordingly, the power of the external loads can be written as:

$$P_{ex} = \Lambda[\alpha \quad \beta \quad \gamma]\boldsymbol{D} \tag{10}$$

In limit analysis a normalization condition is usually prescribed, physically meaning that the shape of the failure mechanism can be identified, but its amplitude is undetermined:

$$[\alpha \quad \beta \quad \gamma]\boldsymbol{D} = 1 \tag{11}$$

In the framework of the upper bound theorem of limit analysis, any point of the homogenized failure surface is determined by means of the following constrained minimization problem:

$$\text{Find min } P_{in} \quad \text{subject to} \begin{cases} [\alpha \quad \beta \quad \gamma]\boldsymbol{D} = 1 & \text{(a)} \\ \mathbf{A}_U^{eq}\mathbf{U} + \mathbf{A}_\lambda^{eq}\dot{\boldsymbol{\lambda}} = \mathbf{0} & \text{(b)} \\ \boldsymbol{D} = \frac{1}{A}\int_{\partial Y} \boldsymbol{v} \overset{s}{\otimes} \mathbf{n} dS & \text{(c)} \\ \dot{\boldsymbol{\lambda}} \geqslant \mathbf{0} & \text{(d)} \end{cases} \tag{12}$$

where (a) is the normalization condition (11), (b) is the set of equations representing the admissibility of the plastic flow, Eq. (6), and (c) links the homogenized strain rate with the local velocity field (see Eq. (1)).

It is interesting to note that the independent variables entering into the optimization problem (12) are the three components of the macroscopic strain rate $\boldsymbol{D}$, the $6 \times 3m$ plastic multipliers $\dot{\boldsymbol{\lambda}}$ and the 7 DOFs defining the microscopic velocity field. Through the normalization condition (11), and equating the internal power dissipation to the power of the external loads, i.e. $P_{ex} = P_{in}$, it can be easily shown that $\Lambda = \min P_{in}$.

Furthermore, it is worth noting that the linear programming problem (12) contains only equality constraints and non-negativity constraints of some variables, a feature which considerably improves the numerical efficiency, especially when sparse matrices are dealt with, as, using an interior-point solution strategy, the recursive factorization of a square submatrix extracted from the set of equality constraints is basically required [38].

3.3. Motivations for the new proposal

From a practical point of view, the main advantages of the present procedure can be summarized as follows:

(a) The actual thickness of the joints is taken into account in a limit analysis procedure involving very few optimization variables (only 7 velocity parameters, plus the collapse multiplier and the plastic multipliers of the sub-cells). Also, the procedure competes favourably – from a computational

point of view – with existing approaches available in the literature to determine the in-plane macroscopic strength domain of masonry directly (see Section 5). It is well known that the reduction of joints to interfaces may result in an overestimate of the macroscopic strength of masonry: the key role played by the thickness of the mortar joints was pointed out e.g. by Mojsilovic and Stewart [39]. This can be easily inferred even from the simple analysis of a vertically compressed wall: taking the compatibility of the transverse strains at the interface between units and bed joints into account leads to the well-known Hilsdorf's failure mechanism [40]. According to Francis et al. [41], if the bed joint thickness increases from 10 to 25 mm, the average compressive strength of masonry decreases by 25% for solid bricks and by 55% for perforated bricks.

(b) The possibility of failure of both the units and the joints can be taken into account. There is no conceptual difference in the implementation of the strength domains of both constituents, each one corresponding to a different sub-cell. Both components are assumed to be in plane-stress conditions. Such assumption is consistent with the reduced thickness of most running bond or header bond masonry walls: its reliability was discussed by Anthoine [42] for various brick patterns. More sophisticated models could be implemented by modifying the failure modes of the unit cell: this will be the object of a future work to incorporate generalized plane-strain conditions in the cases where the plane stress assumption does not apply [42], together with an enriched out-of-plane kinematics [43]. Here, plane stress conditions are assumed, with the aim of showing how this simplifying assumption leads to a strong reduction in the computational cost, improving at the same time the reliability of the solu-tion in comparison with available limit analysis models (see Section 6). Any non-linear strength domain can be adopted for bricks and mortar, even if it is nowadays commonly accepted that a Mohr–Coulomb failure criterion with tension cutoff and limited compressive strength is able to provide quite accurate results for most stress conditions, with a good match with experimental evidences [4]. An extension to 3D kinematics would require the definition of 3D failure criteria for the constituent materials, with an obvious increase in the computation effort, mainly due to the ensuing additional number of plastic multipliers. Too often failure is assumed to be confined in the joints, and the possibility of failure of the units is neglected. This possibility is an important feature of the present procedure. More sophisticated models available in the literature allow for a more precise description of the non-linear behavior of masonry (see e.g. [44,45]): here attention is rather focused on the simplicity and the computational efficiency of the procedure, which are undoubtedly much higher than those of models based on a FE discretization of the unit cell (FEM2 models).

4. Prediction of the compressive strength of wallettes

The uniaxial compressive strength of masonry walls for any orientation ϑ of the head joints to the applied stress (see Fig. 4) was predicted by Ganz [34] and, more recently, by Mojsilovic [35].

To support the theoretical investigations, several experimental results on masonry walls with different brick typologies were obtained at ETH in Zurich (CH) and are partially reported by Ganz [34]. According to his plane-stress failure criterion, Ganz proposed the following formula to evaluate the ultimate vertical load bearing capacity Σ_{22} of masonry wallettes in simple compression, at any angle ϑ:

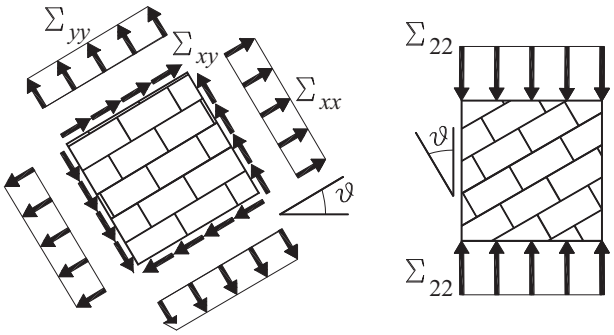

Fig. 4. Masonry element subjected to uniaxial vertical compression (right) and stress components parallel to the joints (left).

$$\Sigma_{22} = \min\left\{\frac{c}{\cos^2\vartheta(\tan\varphi - \tan\vartheta)}, f_x, \frac{2c\cos\varphi}{1-\sin\varphi}\right\} \tag{13}$$

where c and φ are the cohesion and the internal friction angle of the bed joints, and f_x is the uniaxial strength of masonry under horizontal compression.

Recently, Mojsilovic [35] proposed a modification of Ganz's criterion, based on a new failure mode characterized by slip lines along the head joints. Neglecting plastic dissipation in mortar, and assuming the units to be made of a material satisfying Cou-lomb's failure criterion, the anisotropic compressive strength of masonry, Σ_{22}, at any ϑ angle is:

$$\Sigma_{22} = \frac{c_b}{2\sin^2\vartheta(\tan\varphi_b - \cot\vartheta)} \tag{14}$$

where c_b and φ_b are cohesion and internal friction angle of the brick/block material.

In order to test the capabilities of the present MoC approach when compared with the two failure criteria (13) and (14), a running bond masonry wall with thin mortar joints (reduced to interfaces for the sake of simplicity) and standard Italian bricks of height $a = 55$ mm and length $b = 250$ mm is considered. The mechanical properties of the constituent materials in the three models are summarized in Table 1.

In the proposed model, it is necessary to solve the optimization problem (12) to obtain the vertical failure load Σ_{22} for a given orientation ϑ. The coefficients α, β and γ can be easily inferred from Fig. 4 ($\alpha = -\sin^2\vartheta$, $\beta = -\cos^2\vartheta$, $\gamma = -\sin\vartheta\cos\vartheta$).

The law of variation of the anisotropic compressive strength predicted by the present MoC-type model and by those available in the literature [34,35] is depicted in Fig. 5. The predictions of all the models are in good agreement with each other: in particular, the predictions of the MoC-type model closely match those obtained with Mojsilovic's criterion at most orientations.

It is interesting to point out that all models are based on the upper bound theorem of limit analysis. Ganz's and Mojsilovic's formulas, however, are based on prescribed failure mechanisms. It is therefore not surprising that the prediction provided by MoC are more conservative, at least at angles sufficiently lower than 90°.

Whereas the strength values provided by the present approach are obtained numerically (i.e. no closed form solutions are available, unlike in Ganz's and Mojsilovic's approaches), the procedure proposed here is apparently more simple to be used in practical applications, as the masonry strength along the material axes (f_x) has not to be known in advance.

5. Existing homogenization approaches to predict the macroscopic strength domain of masonry

Three alternative homogenization approaches will be used in Section 6 to assess the accuracy of the results provided by the

Table 1
Mechanical properties adopted to predict the anisotropic compressive strength of masonry with different models (brick height = 55 mm, brick length = 250 mm, joints reduced to interfaces).

MoC model						
Mortar					Unit	
f_t (N/mm^2)	f_c (N/mm^2)	Φ_1	Φ_2	c (N/mm^2)	φ_b	c_b (N/mm^2)
0.10	3.0	36°	30°	0.10	40	1
Ganz (1985) and Mojsilovic (2011) models						
c (N/mm^2)	φ	f_y (N/mm^2)	c_b (N/mm^2)	φ_b		
0.1	36°	3.2	1	40		

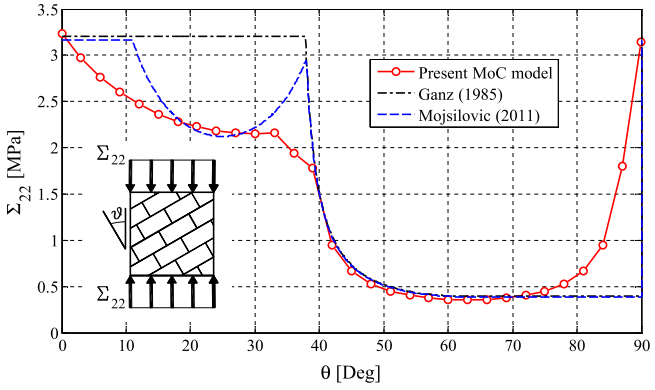

Fig. 5. Comparison among the uniaxial compressive strength at different orientations of the head joint to the applied stress predicted by the present model and by Eqs. (13) and (14).

proposed approach. In particular, two procedures based on the lower bound theorem of limit analysis [22,27] and one based on the upper bound theorem [26] are briefly recalled hereafter; their pros and cons are also highlighted.

The first approach is based on the lower bound theorem of limit analysis. The unit cell is divided into a limited number of rectangular sub-domains, see Fig. 6, and a polynomial interpolation of degree m of the stress field within each element is a priori proposed. Any stress component in the kth sub-domain Y^k is expressed as

$$\sigma_{ij}^{(k)} = \mathbf{X}(\mathbf{y})\mathbf{S}_{ij}^T \quad \mathbf{y} \in Y^k,$$

where $\mathbf{X}(\mathbf{y}) = [1 \quad y_1 \quad y_2 \quad y_1^2 \quad y_1y_2 \quad y_2^2 \quad \dots]$ and $\mathbf{S}_{ij} = [S_{ij}^{(1)} \quad S_{ij}^{(2)} \quad S_{ij}^{(3)} \quad S_{ij}^{(4)} \quad S_{ij}^{(5)} \quad S_{ij}^{(6)} \quad \dots]$ is an array of $\widetilde{N} = 1/2\,(m+1)\,(m+2)$ entries representing the unknown stress parameters. Equilibrium within each element and at the interface between contiguous elements, as well as anti-periodicity conditions for the stress vector, are a priori imposed to reduce the number of optimization parameters.

In [22] four models, labeled P0, P2, P3 and P4 and corresponding to a constant, quadratic, third- and fourth-order polynomial approximation of the micro-stress field, respectively, have been presented and tested. P0 was shown to be unable to capture the material orthotropy. P2 predicts different strengths along the material axes, but the approximation is affected by errors exceeding 10%, if compared with the solution obtained by FEs. P3 furnishes satisfactory results needing a relatively reduced time for the evaluation of the failure surface. P4 is the most accurate model, but at the same time requires a huge computational effort.

The most interesting feature of this static approach is likely to be the possibility of taking the actual thickness of the joints into account, the importance of which has already been emphasized (see Section 3.3 and [39]).

The second approach, presented in [27], relies upon a subdivision of the unit cell into 24 constant stress triangular elements; joints are reduced to interfaces (see Fig. 7). Adding suitable constraints, the stress field within the RVE fulfils equilibrium equations (with vanishing body forces) and periodicity conditions. According to the lower bound theorem of limit analysis, and thanks to the rough discretization adopted, a safe approximation of the macroscopic strength domain under biaxial stress states can be obtained without resorting to any computer. Readers are referred to the original paper [27] for more detail.

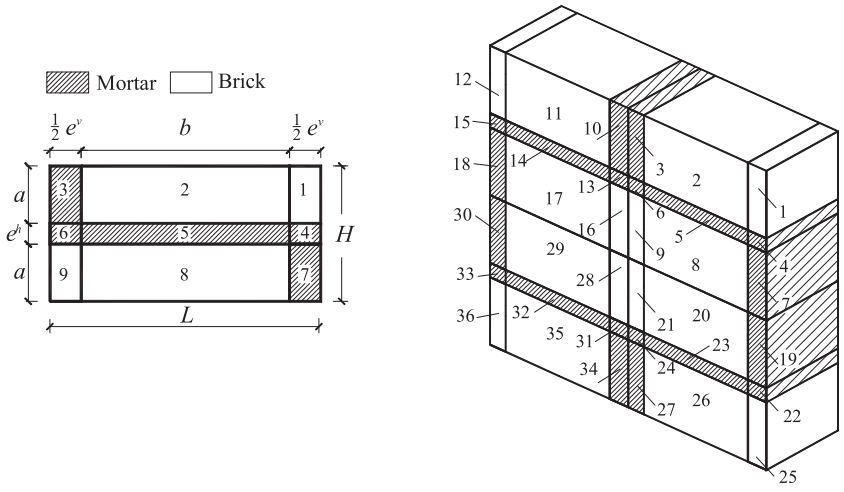

Fig. 6. Equilibrated approach proposed in [22]. Left: subdivision and geometrical characteristics of one-fourth of the elementary cell. Right: subdivision of the entire cell into 36 sub-domains.

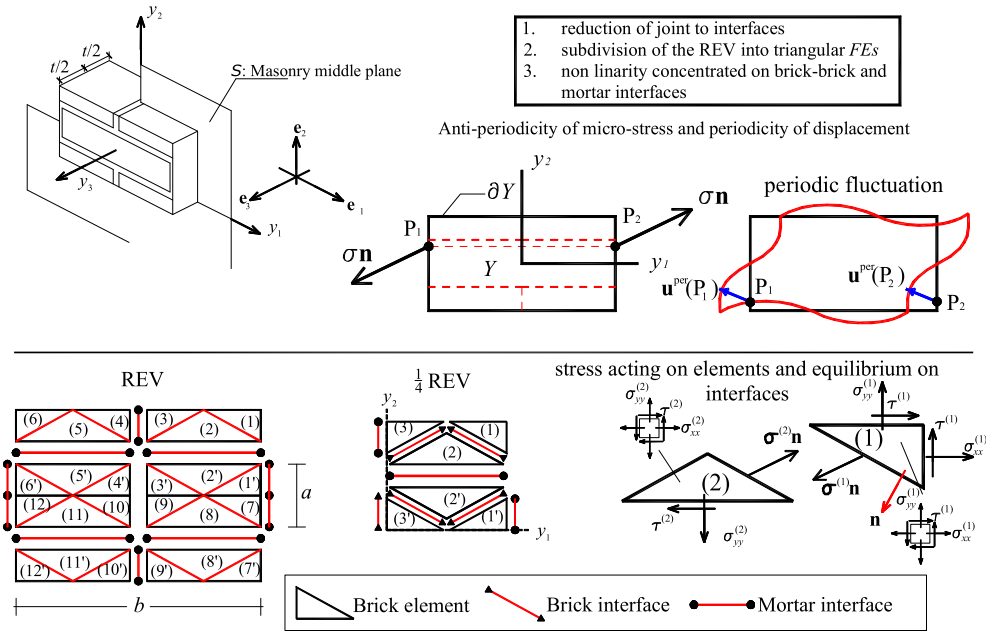

Fig. 7. The micro-mechanical model proposed. Subdivision of the RVE into 24 CST triangular elements (and 1/4 into 6 elements) and anti-periodicity of the micro-stress field.

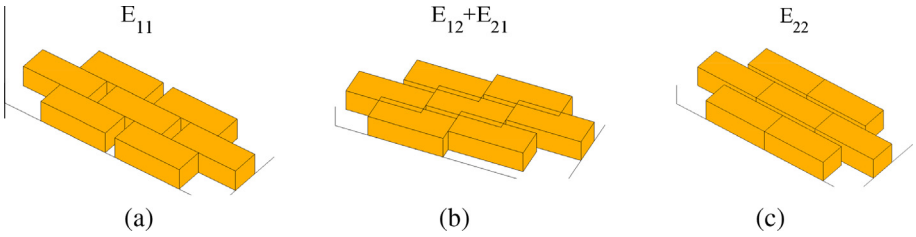

Fig. 8. Deformation modes considered in the compatible identification model [26].

An intrinsic limitation of this approach is the need of reducing joints to interfaces. As it will be shown in the following sections, such assumption leads to overestimate the actual macroscopic strength of masonry, especially under uniaxial horizontal tension/compression.

The last approach used for validation relies upon the so-called "compatible identification model" [26]. In this model, bricks are supposed to be infinitely strong, whereas joints are reduced to interfaces obeying a Mohr–Coulomb failure criterion with tension cut-off and limited compressive strength. A sub-class of possible elementary deformation modes is a priori defined for the unit cell, with the aim of capturing cracking of the joints. For the sake of illustration, Fig. 8 shows the deformation modes of the elementary cell undergoing macroscopic stretching along the bed joints (a), along the head joints (c), and in-plane shear (b). Owing to its kinematic nature, this approach gives an upper bound to the macroscopic strength domain of masonry. Again, readers are referred to the original paper [26] for additional information about the model.

The main advantage of the procedure proposed in [26] is its simplicity, which allows the macroscopic failure surface to be determined quite straightforwardly. The total number of optimization variables is very limited, and basically consists of the parameters defining the rigid motion of the blocks and the plastic multipliers of the interfaces. The major limitations lie in the assumptions underlying the model (infinite strength of the blocks, negligible thickness of the joints). Finally, note that the lower bound [27] and the upper bound [26] coincide if the assumptions underlying the compatible identification model apply, meaning that in this case the actual homogenized failure surface can be exactly determined.

6. Homogenized strength domain and comparisons with the existing literature

The kinematic limit analysis approach described in Section 3 will be now applied to derive the macroscopic strength domain of masonry under in-plane macroscopic principal stresses acting at any orientation to the bed joints. The theoretical predictions given by the three approaches recalled in Section 5 and available in the literature will also be shown for validation purposes.

Since the first approach (based on a polynomial expansion of the microscopic stress field [22]) has the advantage of explicitly taking the real thickness of the joints into account, similarly to the approach proposed in this work, it can be conveniently employed to estimate the discrepancy with the predictions of the MoC-type approach (which gives an upper bound to the macro-scopic strength domain) for joints of finite thickness. According to the authors' experience, the proposed model always requires a little fraction of the time required by [22] to provide good estimates of the homogenized failure surface, owing to the very limited number of unknowns involved. Since the MoC-type approach gives an upper bound to the real macroscopic strength domain and the polynomial expansion of the micro-stress field gives a lower bound, the classic theorems of limit analyses ensure that the real macroscopic failure surface lies somewhere between the

two predictions. As it will be shown hereafter, these predictions do not differ significantly from an engineering point of view, so that the estimation given by the MoC can be used for practical purposes.

The second approach (based on a rough discretization of the RVE into CST elements [27]) and the third one (or compatible identification approach [26]) predict the same failure surface when bricks are assumed to be infinitely strong, and can be useful to assess (1) the applicability of the MoC-type approach to extremely thin joints and (2) the role played by the joint thickness on the masonry homogenized strength domain. Incidentally note that, as the equilibrated CST model is based on the lower bound theo-rem and the compatible identification model on the upper bound theorem, the homogenized failure surface is exactly determined in case of joints reduced to interfaces and infinitely resistant units.

The upper bound to the macroscopic failure surface given by the MoC for brickwork with sufficiently thin joints and units much stronger than mortar is expected to match that given by both approaches.

Table 2
Mechanical properties adopted for mortar in the numerical prediction of the homogenized failure surface.

Friction angle (Φ)	Cohesion (c)
36°	0.1 MPa
$f_t = \frac{2c\cos(\Phi)}{1+\sin(\Phi)}$	$f_c = \frac{2c\cos(\Phi)}{1-\sin(\Phi)}$

In the applications shown in this section, running bond masonry consisting of standard Italian bricks (250 × 120 × 55 mm^3 in size) and 10 mm thick joints is considered. Bricks are assumed to be infinitely strong, whereas mortar is supposed to obey a Mohr–Coulomb failure criterion, defined by the parameters summarized in Table 2. Accordingly, the tensile and compressive strengths of the joints, f_t and f_c, are given by the relations reported in Table 2. Therefore, to make the analysis with joints of finite thickness consistent with those carried out with joints of vanishing thickness (e.g. [24,26]), the Mohr–Coulomb strength criterion of the interfaces is complemented by a compression cap and a tension cut-off, with values equal to f_c and f_t, respectively.

In Fig. 9, a comparison is made among the failure surfaces obtained in biaxial tension using the MoC-type approach, and the homogenization models recalled above. In particular, Fig. 9a refers to the polynomial expansion model proposed in [22], Fig. 9b to both the equilibrated CST model presented in [24] and the upper bound compatible identification model proposed in [28], and Fig. 9c to the present model. Σ_{xx} and Σ_{yy} (= Σ_{xx} tgψ) denote the two nonvanishing macroscopic principal stresses. Σ_{xx} is supposed to act at θ = 0°, 22.5° or 45° to the bed joints (i.e. to y_1, see Fig. 1a). When dealing with the polynomial expansion approach, a cubic interpolation of the stress field (P3 model) is adopted, as it is a good compromise between computational efficiency and accuracy (which both increase with the degree of the polynomial interpolation).

The dependence of the homogenized failure surfaces from the joint thickness can also be inferred from Fig. 9, by comparing, for

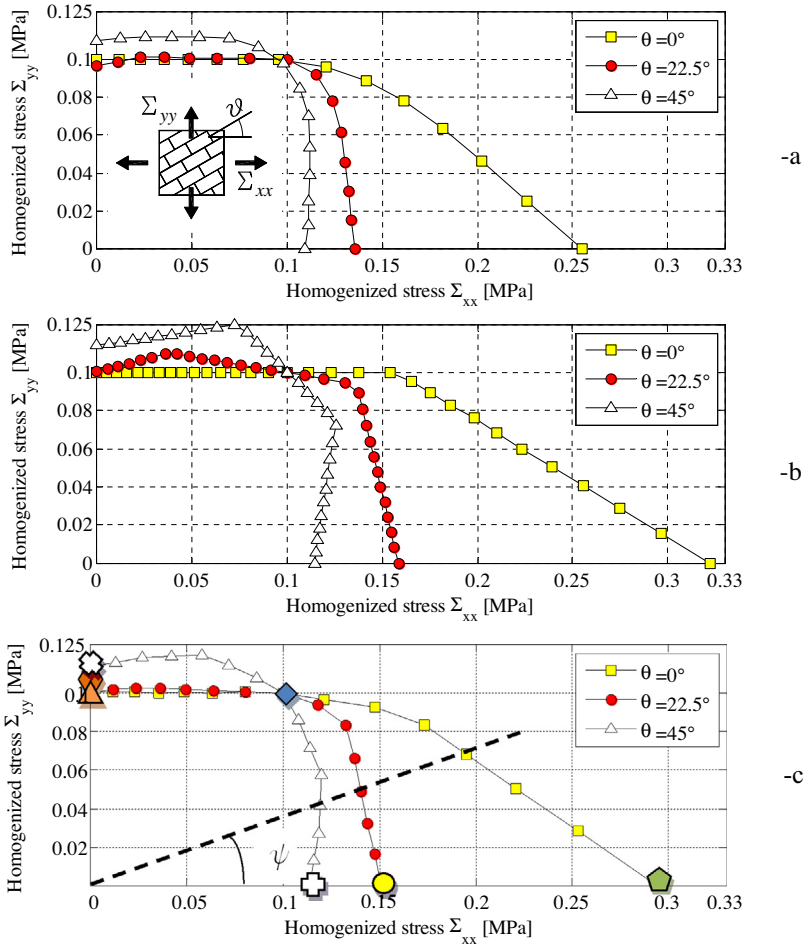

Fig. 9. Comparison among the results given by the different homogenization models under biaxial tension for the masonry material of Table 2. (a) Polynomial expansion of the stress field, P3 approach. (b) Equilibrated CST discretization and "compatible identification model". (c) MoC-based model.

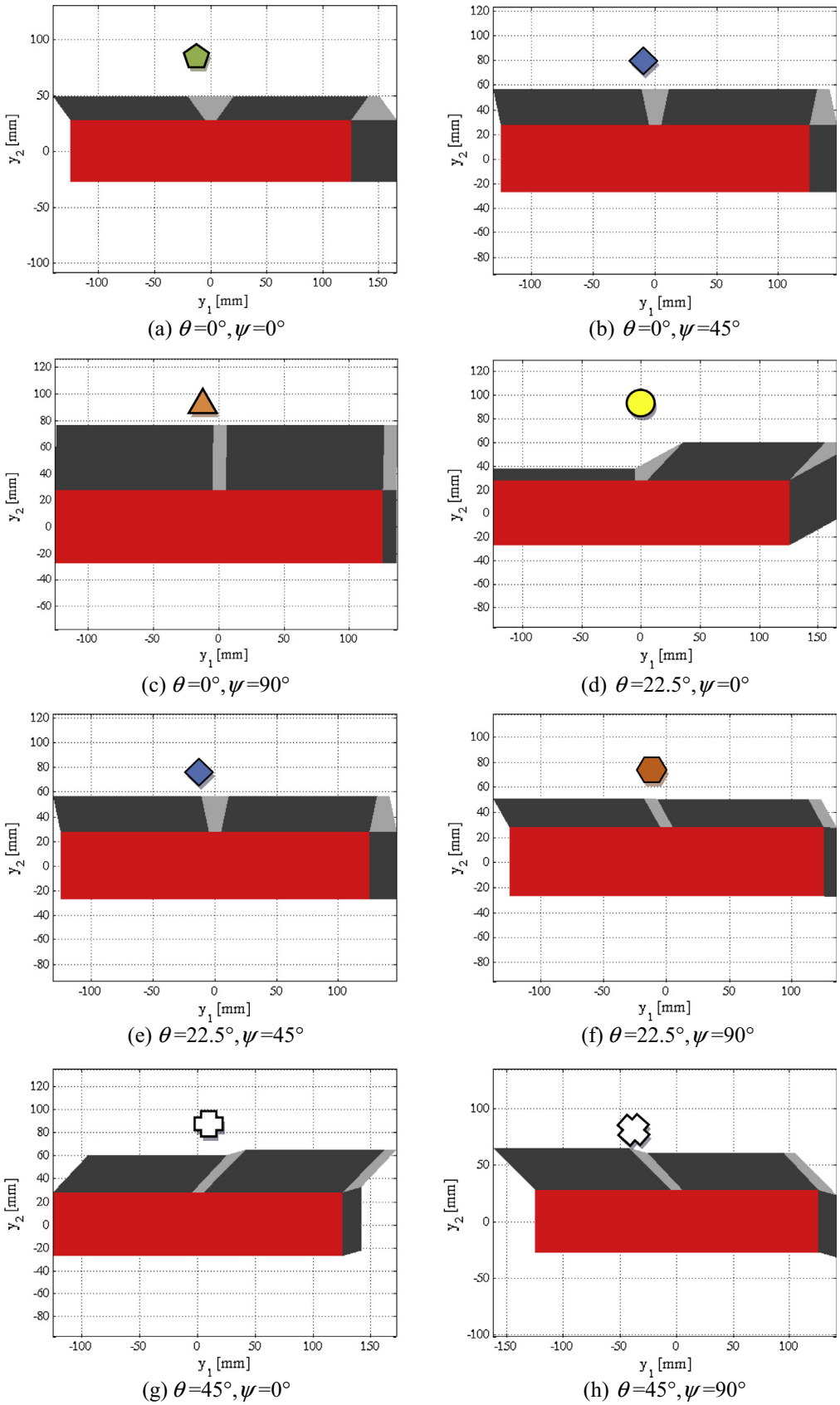

(a) θ=0°, ψ=0°

(b) θ=0°, ψ=45°

(c) θ=0°, ψ=90°

(d) θ=22.5°, ψ=0°

(e) θ=22.5°, ψ=45°

(f) θ=22.5°, ψ=90°

(g) θ=45°, ψ=0°

(h) θ=45°, ψ=90°

Fig. 10. RVE failure modes corresponding to the points indicated in Fig. 9c ($tg\psi = \Sigma_{yy}/\Sigma_{xx}$).

instance, subfigures c and b. Thick joints correspond to smoother failure surfaces (Fig. 9c). Conversely, in case of joints reduced to interfaces the failure surface coincides with the boundary of the multi-plane strength domain proposed by de Felice and de Buhan [20].

According to all of the models, the highest strength under horizontal tension is attained at $\theta = 0°$, and is much lower in the case of thick joints (0.26 MPa) than in presence of infinitely thin joints (0.31 MPa), with a percent difference of about 15%.

Fig. 10 shows the failure modes of the RVE predicted by the MoC, corresponding to the points denoted by the same symbol in Fig. 9c. For the sake of illustration, the deformed shape of the RVE at $\theta = 0°$ and $\psi = 0^{\circ}$ (simple horizontal tension, Fig. 10a) shows that, in agreement with the results provided by alternative homogenization models, head joints are subjected to simple tension, whereas bed joints undergo pure shear. Cross joints, conversely, exhibit a mixed mode failure, which however has little influence on the value of the homogenized strength as their size is small. It is interesting to notice how, in most cases, bed joints fail in shear or for a mixed mode: accordingly, the macroscopic tensile strength along the horizontal direction ($\theta = 0°$ and $\psi = 0^{\circ}$) is sensibly higher than that under vertical tension ($\theta = 0°$ and $\psi = 90^{\circ}$), when the bed joint fails in simple tension (Fig. 10c).

Finally, when joints are reduced to interfaces, the MoC model gives results in perfect agreement with the compatible identification model and the CST equilibrated model (see Fig. 11). This shows the good predictive capabilities of the MoC-type approach even for extremely thin joints.

In order to closely bracket the actual homogenized failure surface in case of joints of finite thickness, it is possible to compare the results obtained with the MoC-type approach (upper bound to the real macroscopic strength domain) with those provided by the polynomial expansions of the micro-stress field (lower bounds), at increasing degrees of the polynomials (P2 to P4). In Fig. 12, three sections of the failure surface under biaxial tension (at $\theta = 0°$, 22.5° or 45°) are shown. Comparing Fig. 12c and d, the MoC and the P4 model are found to provide very similar results, the maximum difference being obtained at $\theta = 0°$ under horizontal tension (about 7%).

The same type of comparison is repeated under biaxial compression: the results, normalized to the compressive strength of the mortar joints f_c, are reported in Fig. 13. Again, the agreement between P4 and MoC models appears to be rather satisfactory, with negligible differences from an engineering viewpoint.

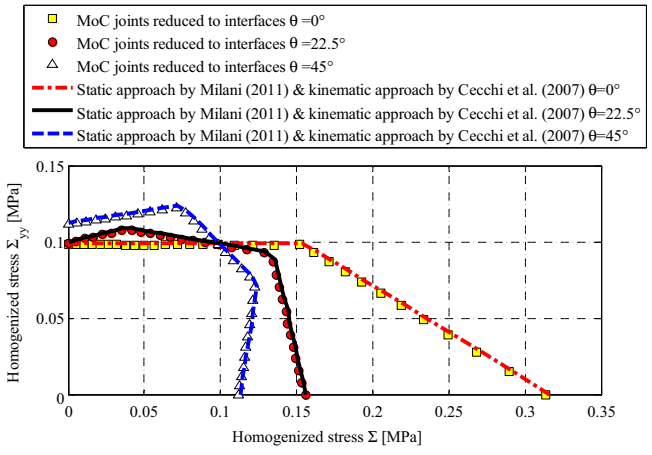

Fig. 11. Comparison between the results of the MoC-type approach and those of the static [27] or kinematic [26] approaches available in the literature for the masonry material of Table 2 under biaxial tension.

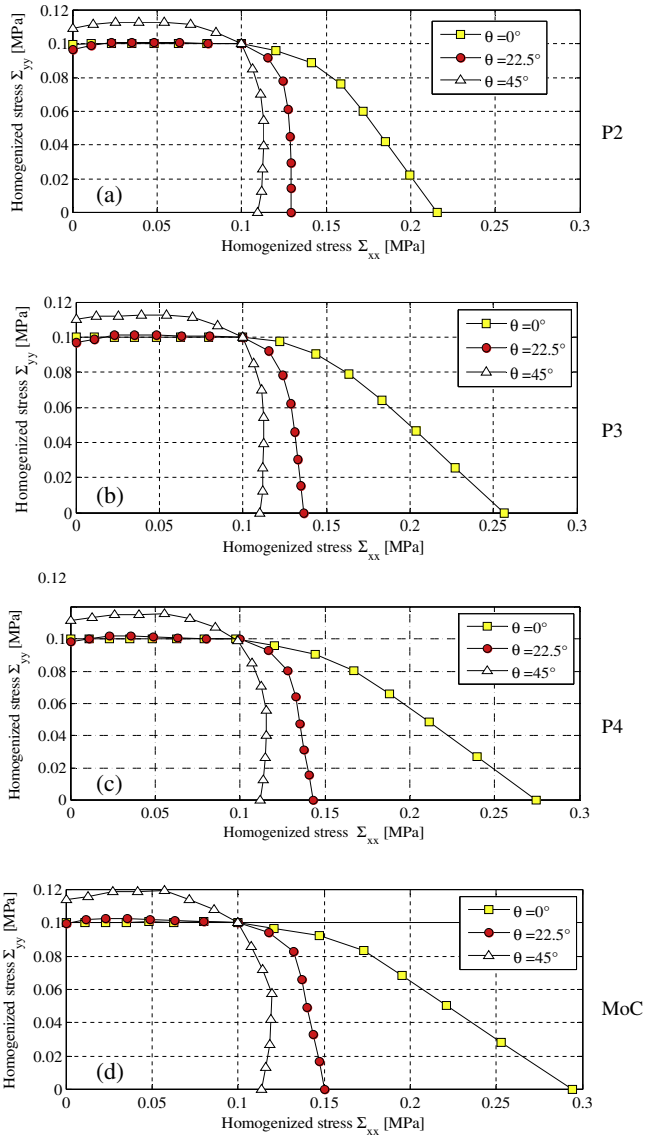

Fig. 12. Comparison between homogenized failure surfaces predicted by the lower bound polynomial approximations (a–c) and by the MoC-type upper bound (d) under biaxial tension, using the mechanical properties of Table 2.

7. Comparison with experimental data in biaxial compression

To assess the predictive capabilities of numerical and analytical homogenization models for masonry under biaxial stress at failure, most authors refer to the experimental data set of Page [46].

Here, reference is made to similar biaxial compression tests, conducted by Papa and Nappi [36] at the Technical University (Politecnico) of Milan, Italy. The authors preferred to compare their predictions with these tests, as they had full access to the experimental results. Papa and Nappi [36] tested 180 panels of 1:4 scale solid clay brick masonry with dimensions $200 \times 200 \times 30\ mm^3$ (cut from $275 \times 235 \times 30\ mm^3$ miniaturized panels previously built by means of convenient moulds). The dimensions of the units were $65 \times 30 \times 25\ mm^3$ and the joint thickness was 5 mm. The panels were loaded increasing the principal stresses Σ_{xx} and Σ_{yy} proportionally, at different orientations θ with respect to the material axes (see Fig. 9a).

The material properties of mortar and units adopted are given in Table 3. For both components a Mohr–Coulomb failure criterion with tension cut-off and a multi-linearized elliptic cap in

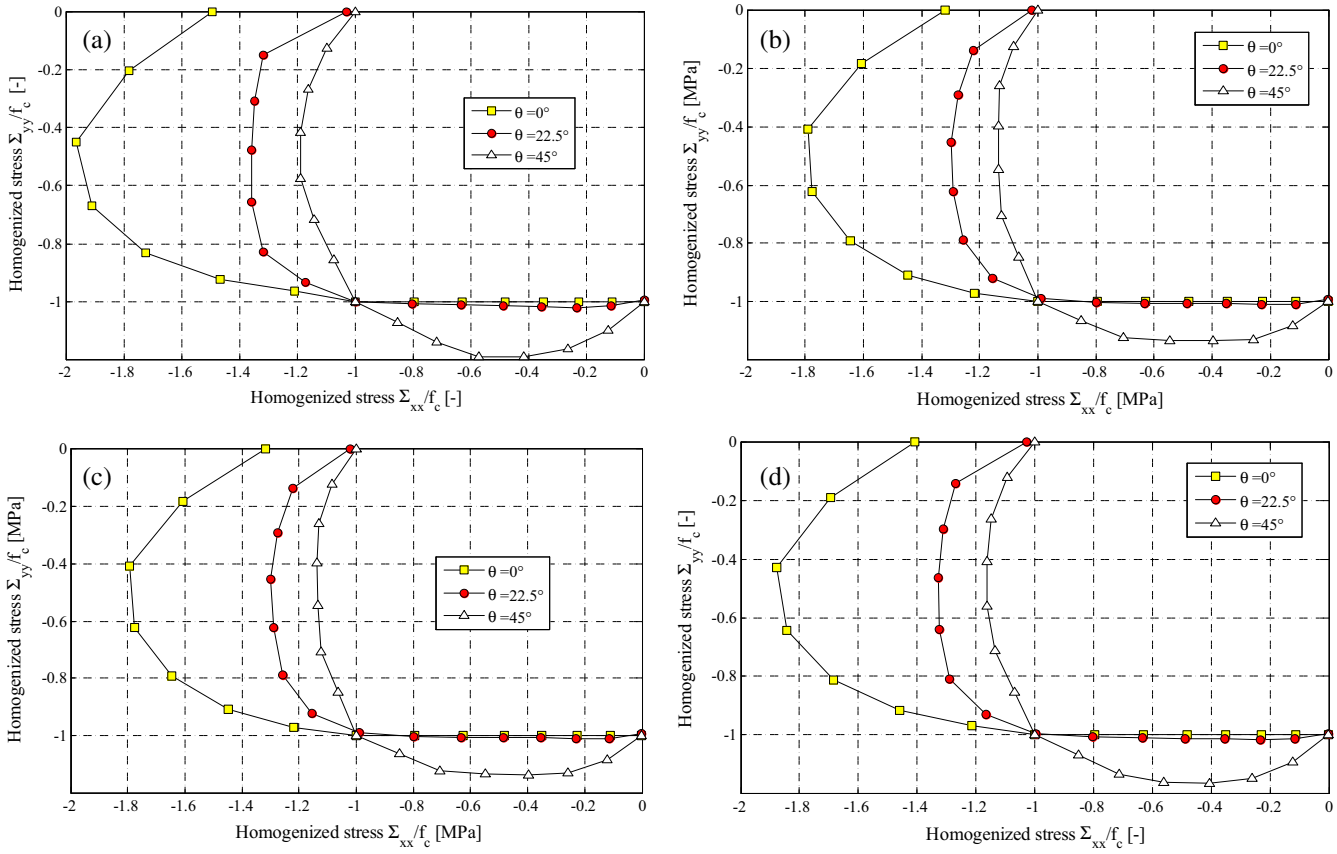

Fig. 13. Comparison between polynomial lower bounds and MoC upper bound to the macroscopic failure surface under biaxial compression; mechanical properties of Table 2. (a) MoC. (b) P2. (c) P3. (d) P4.

Table 3
Strength parameters used to fit the experimental data of Papa and Nappi [36].

f_t (N/mm^2)	f_c (N/mm^2)	Φ_1 (°)	Φ_2 (°)	c (N/mm^2)
Mortar				
1.1	21.2	37	30	$1.0f_t$
Units				
2.0	23.0	60	45	$1.5f_t$

compression is assumed. It is worth noting that in [36] no detailed information on the mechanical properties of the constituent materials (such as cohesion, friction angle and tensile strength) is provided. Only brick and mortar compressive strengths are reported, which are not sufficient to fully identify all the strength parameters. Accordingly, the values of some of these parameters were simply determined by best fitting the experimental data.

In Table 3, for each constituent f_t denotes the uniaxial tensile strength, f_c the compressive strength, c the cohesion, Φ_1 is the friction angle and Φ_2 the angle between the tangent to the elliptic cap at zero shear stress and the σ-axis in Mohr's plane.

In Fig. 14 the homogenized failure surfaces at $\theta = 0°$, 30° and 45° are reported and compared with the experimental data. On account of the experimental scatter, the numerically obtained failure surfaces fit the experimental data reasonably well.

In Fig. 15, a comparison between numerically determined and experimentally observed failure modes is provided for some meaningful stress conditions. The deformed shape of the elementary cell is suitably replicated several times, in order to clearly represent the behavior at failure of a small *quasi*-square wallette constituted by 3.5 and by 10 bricks along the horizontal and the vertical direction, respectively. Each failure mode is identified by a geometric symbol, reported also on the failure surfaces in Fig. 14. In simple vertical compression, the wallette is experimentally found to fail due to the formation of vertical cracks crossing both joints and bricks: this failure mode is matched by the straight yield line observed in the numerical simulations (Fig. 15a). A similar behavior is experienced in the numerical model under horizontal compression (Fig. 15b), although also the bricks are found to fail in compression unlike the experimental evidences. Shear failure is also visible in the bed joints both numerically and experimentally under off-axis compression at $\theta = 30°$ (Fig. 15c), whereas a yield line involving both mortar and bricks characterizes the failure mechanism at $\theta = 45°$ (Fig. 15d), with a good agreement between experiments and numerical simulations.

8. The limit analysis problem at the structural level

The upper bound FE heterogeneous and homogenized limit analysis approach adopted at a structural level bases on a triangular discretization with linear interpolation of the velocity field inside each element. Possible velocity jumps can occur at the interfaces between contiguous elements, in agreement with the FE code originally proposed by Sloan and Kleeman [47]. Indeed, whereas in the present work the microscopic velocity field is continuous within each RVE (Section 3), discontinuities in the macroscopic velocity field over any structure are allowed. This is required to capture the failure mechanisms of most structural elements consisting of masonry-like materials, which area characterized by cracks or slip surfaces.

Two different approaches are proposed hereafter to estimate the limit load of masonry structures. In the heterogeneous approach, assuming a finite thickness of the joints, triangular elements

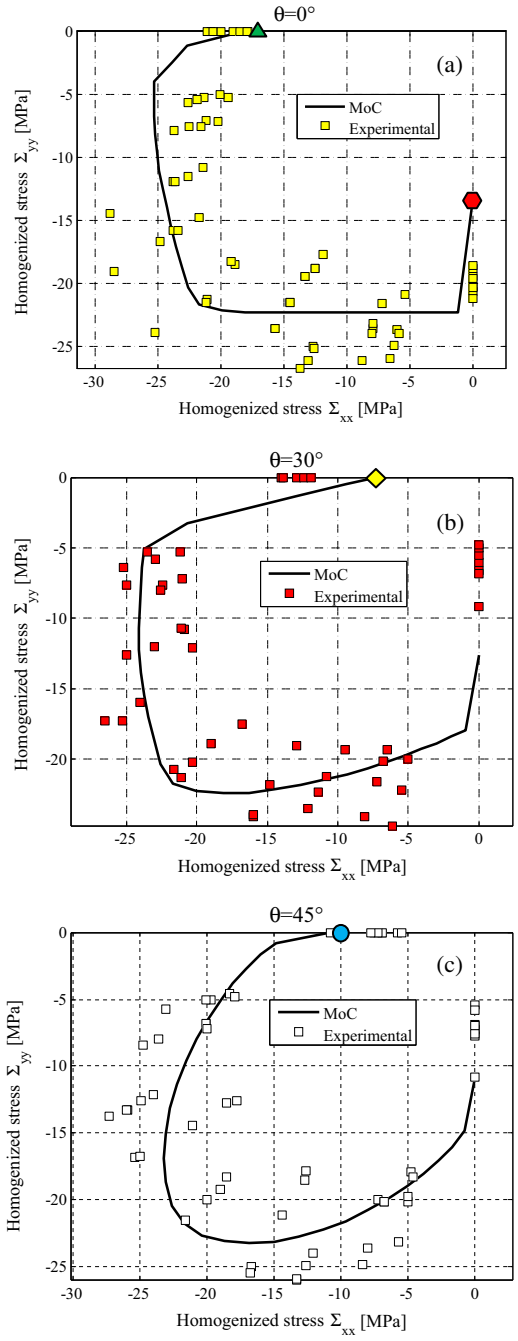

Fig. 14. Comparison between theoretical predictions (MoC-type model) and experimental data [36] under biaxial compression.

represent either mortar or bricks, and the interfaces between bricks and mortar are assumed to have the mechanical properties of mortar for the sake of simplicity. In the homogenized approach, the body is subdivided into triangles without any reference to the real pattern, with jumps in velocity allowed along the interfaces, having the mechanical properties of the homogenized material.

The finite element implementation of the upper bound theorem of limit analysis leads to a linear programming problem in which the total dissipated internal power has to be minimized subject to equality and inequality constraints. Equality constraints include compatibility, plastic flow within the elements and at the interfaces, and boundary conditions. In more detail, for any pair of nodes (labeled 1 and 2 hereafter – see Fig. 16b) on the interface between two adjacent triangles M and N, the jump in tangential and normal velocity, $\Delta\mathbf{v}$, can be written in terms of the Cartesian nodal velocities of the elements (see Fig. 16 and [23,47] for details). Four linear equations of the form:

$$\mathbf{A}_{11}^{eq}\mathbf{v}^{M} + \mathbf{A}_{12}^{eq}\mathbf{v}^{N} + \mathbf{A}_{13}^{eq}\Delta\mathbf{v} = \mathbf{0} \tag{15}$$

can be written for each interface, where $\mathbf{v}^M$ and $\mathbf{v}^N$ are the 6×1 arrays collecting the Cartesian nodal velocities of element M and N, respectively, $\mathbf{A}_{11}^{eq}$ and $\mathbf{A}_{12}^{eq}$ are 4×9 matrices depending on the nodal coordinates of the elements, and $\mathbf{A}_{13}^{eq}$ is a 4×4 matrix depending only on the coordinates of nodes 1 and 2.

Within each element, three equality constraints representing the plastic flow in continuum (obeying an associated flow rule) are introduced, of the form:

$$\dot{\boldsymbol{\varepsilon}}_{pl}^{E} = \begin{bmatrix} \frac{\partial v_x}{\partial x} & \frac{\partial v_y}{\partial y} & \frac{\partial v_y}{\partial x} + \frac{\partial v_x}{\partial y} \end{bmatrix} = \dot{\lambda}^{E} \frac{\partial S^{C}}{\partial \boldsymbol{\Sigma}^{C}} \tag{16}$$

where $\dot{\boldsymbol{\varepsilon}}_{pl}^{E}$ is the array gathering the plastic strain rate components of element E, $\dot{\lambda}^{E} \geqslant 0$ is the plastic multiplier rate, S^C denotes the continuum failure surface, and $\boldsymbol{\Sigma}^{C} = [\,\sigma_x \quad \sigma_y \quad \tau\,]^{T}$ collects the non-vanishing Cartesian stress components in plane stress conditions within the continuum.

The failure surface is, in general, nonlinear, both in the homogenized and in the heterogeneous case. Assume that a linearization with p planes of the failure domain, of the form $S^{C} \equiv \mathbf{A}^{in}\boldsymbol{\Sigma}^{C} \leqslant \mathbf{b}^{in}$, is available, where $\mathbf{A}^{in}$ is a $p \times 3$ matrix and $\mathbf{b}^{in}$ a $p \times 1$ array: each row of the matrix inequality defines a half-space in the stress space containing the origin. Three linear equality constraints per element can be written in the form:

$$\mathbf{A}_{21}^{eq}\mathbf{v}^{E} + \left(\mathbf{A}^{in}\right)^{T}\dot{\boldsymbol{\lambda}}^{E} = \mathbf{0} \tag{17}$$

where $\mathbf{v}^E$ is the 3×1 array of the element velocities, $\dot{\boldsymbol{\lambda}}^{E}$ is the $p \times 1$ array of the plastic multiplier rates of the element (one for each plane of the linearized failure surface), and $\mathbf{A}_{21}^{eq}$ is a 3×6 matrix depending only on the nodal coordinates of the element.

Similarly to the continuum case, the linearized failure domain for the interfaces (i.e., brick-to-brick, mortar-to-mortar or mortar-to-brick interfaces when a heterogeneous approach is adopted; interfaces between adjacent elements in the homogenized approach) can be cast in the form $S^{I} \equiv \mathbf{A}_{I}^{in}\boldsymbol{\Sigma} \leqslant \mathbf{b}_{I}^{in}$. Here $\boldsymbol{\Sigma} = [\,\sigma \quad \tau\,]^{T}$ collects the normal stress and the shear stress acting on the interface, whereas $\mathbf{A}_{I}^{in}$ and $\mathbf{b}_{I}^{in}$ define any linearization plane.

Once the interface failure surfaces are linearized, the jump in velocity across the discontinuities is computed introducing the rates of the plastic multipliers for each interface I as follows:

$$\Delta\mathbf{v}(\xi) = \begin{bmatrix} \Delta v_n(\xi) \\ \Delta v_t(\xi) \end{bmatrix} = \sum_{i=1}^{m} \dot{\lambda}_{I}^{(i)}(\xi)\nabla f_{\boldsymbol{\sigma}}^{(i)} \tag{18}$$

where

- ξ is a local coordinate defined along the interface, ranging between 0 and 1;
- $\nabla f_{\boldsymbol{\sigma}}^{(i)}$ are constant gradients for the failure surface ($f^{(i)}$ being the ith segment the 2D multi-linear failure surface consists of);
- $\dot{\lambda}_{I}^{(i)}$ are the interface plastic multiplier rates, evaluated at ξ and associated with the ith segment of the multi-linear failure surface;
- Δv_n and Δv_t are the normal and tangential components of the velocity jump across the discontinuities, respectively.

In the classic kinematic approach of limit analysis a normalization condition for the external power is needed, providing a further equality constraint of the form:

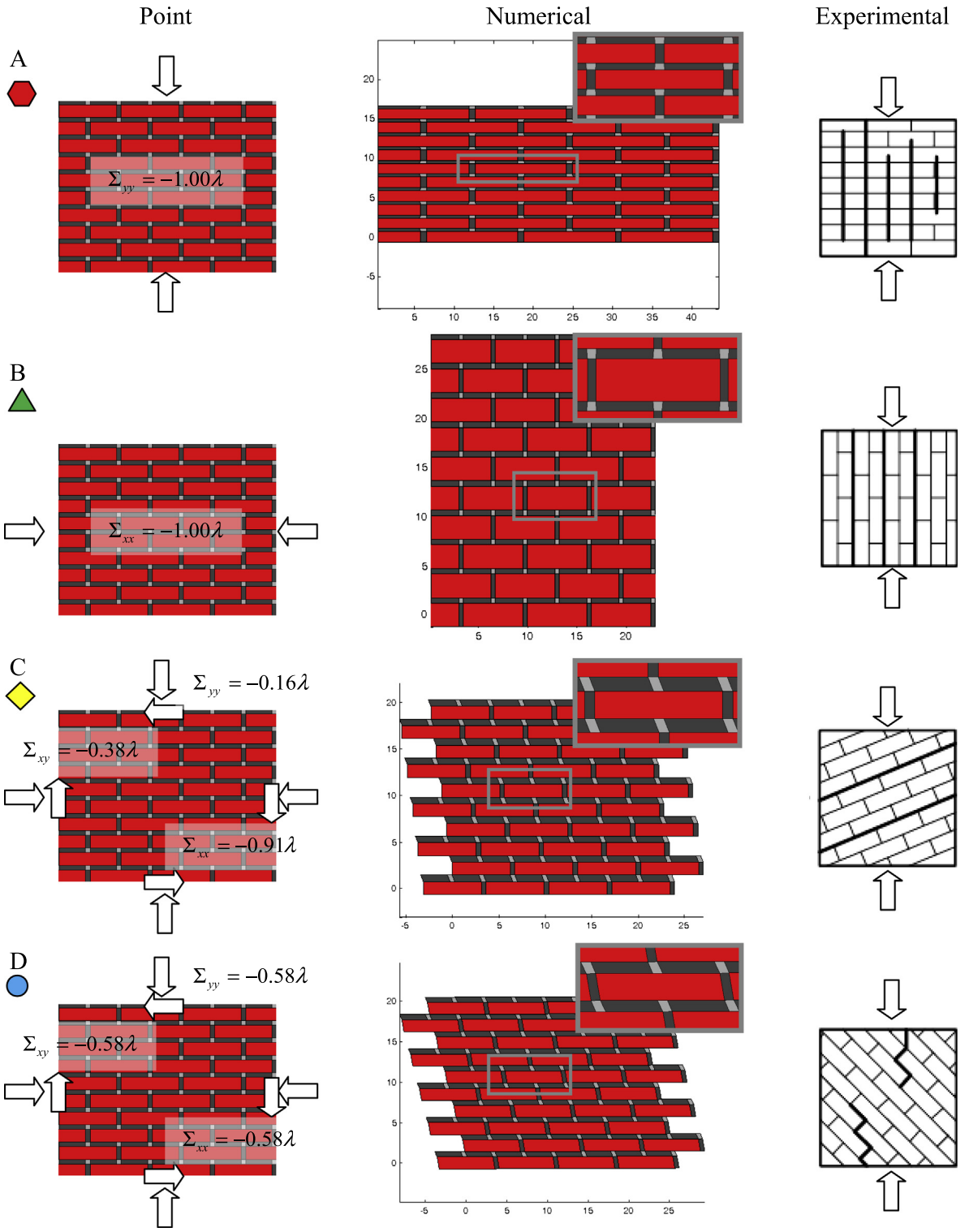

Fig. 15. Comparison between numerical and experimentally observed failure modes for some meaningful points of the strength domain of Fig. 14.

$$\boldsymbol{A}_n^{eq} v = 1 \tag{19}$$

where $\mathbf{A}_n^{eq}$ is a $1 \times 6n^{\mathrm{el}}$ (n^{el}: number of elements) matrix and $\boldsymbol{v}$ is the array of the assembled element nodal velocities.

After some elementary assemblage operations, a simple linear programming problem is obtained (analogous to that reported in [23,47]) in which the objective function to be minimized is the total internal dissipated power P:

$$\begin{cases} \min P = \left(\mathbf{b}_a^{in}\right)^T \dot{\boldsymbol{\lambda}}_E^a + \left(\mathbf{b}_{l,a}^{in}\right)^T \dot{\boldsymbol{\lambda}}_l^a \\ \text{such that} \begin{cases} \mathbf{A}^{eq}\mathbf{U} = \mathbf{b}^{eq} \\ \dot{\boldsymbol{\lambda}}_E^a \geqslant 0 \\ \dot{\boldsymbol{\lambda}}_l^a \geqslant 0 \end{cases} \end{cases} \tag{20}$$

where

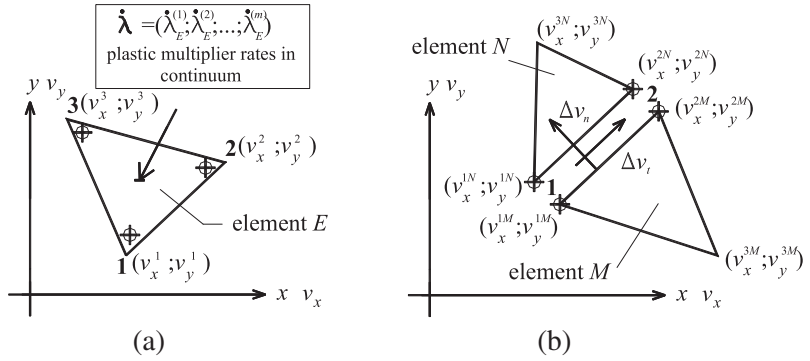

Fig. 16. Triangular element used in the upper bound FE limit analysis problem (a) and jump in velocity across any interface between adjacent triangles (b).

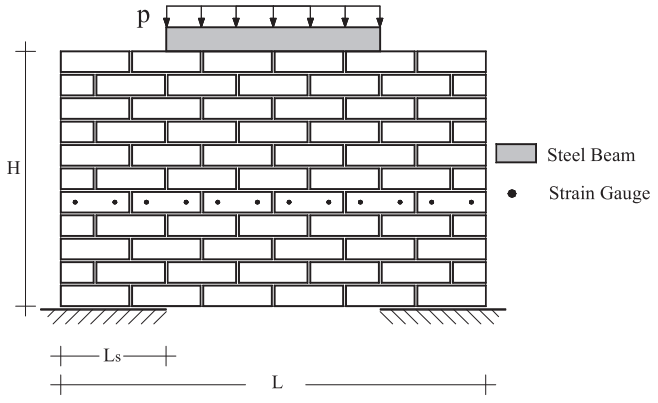

Fig. 17. Geometry and boundary conditions for the deep beam tested by Page [54]: L = 754 mm, H = 457 mm, L_s = 188 mm.

- $\mathbf{b}_a^{in}$ and $\mathbf{b}_{I,a}^{in}$ are the assembled right-hand sides of the inequalities, which define the linearized failure domain of the continuum material and of the interfaces, respectively;
- $\mathbf{U} = \left[\boldsymbol{v} \quad \dot{\boldsymbol{\lambda}}_E^a \quad \Delta \boldsymbol{v}^a \quad \dot{\boldsymbol{\lambda}}_I^a\right]$ is the array of the assembled unknown variables, which collects the element nodal velocities ($\boldsymbol{v}$), the plastic multiplier rates of all the elements ($\dot{\boldsymbol{\lambda}}_E^a$), the velocity jumps across all the interfaces ($\Delta \boldsymbol{v}^a$), and the plastic multiplier rates of all the interfaces ($\dot{\boldsymbol{\lambda}}_I^a$);
- $\mathbf{A}^{eq}$ is the matrix gathering the coefficients of the overall constraints, and collects velocity boundary conditions, relations between velocity jumps across interfaces and elements velocities, Eq. (15), constraints for plastic flow in continuum, Eq.(17), constraints for plastic flow in velocity discontinuities, Eq.(18), and normalization condition, Eq. (19).

It is worth noting that the objective function P consists of two contributions, representing the total power dissipated within the continuum, $P^E = \left(\mathbf{b}_a^{in}\right)^T \dot{\boldsymbol{\lambda}}_E^a$, and that dissipated at the interfaces, $P^I = \left(\mathbf{b}_{I,a}^{in}\right)^T \dot{\boldsymbol{\lambda}}_I^a$. Within each triangle E of area A_E, writing the expression of each of the p planes linearizing the failure surface as $\mathbf{A}^{in}(q,1)\sigma_x + \mathbf{A}^{in}(q,2)\sigma_y + \mathbf{A}^{in}(q,3)\tau = \mathbf{b}^{in}(q)$, $q = 1, \ldots, p$, it can be shown that the dissipated power is:

$$P^E = A_E \sum_{q=1}^{p} \mathbf{b}^{in}(q) \dot{\lambda}_E^{(q)} \tag{21}$$

where $\dot{\lambda}_E^{(q)}$ is the plastic multiplier rate of triangle E associated with the qth plane.

Similarly, within each interface I of length Γ_I, supposing that the linearized strength domain is bounded by p^I straight lines of the form $\mathbf{A}_I^{in}(q,1)\sigma + \mathbf{A}_I^{in}(q,2)\tau = \mathbf{b}_I^{in}(q)$, $q = 1, \ldots, p^I$, the dissipated power reads:

$$P^I = \Gamma_I / 2 \sum_{q^I=1}^{m^I} b_I^{in} \left(\dot{\lambda}_{I,1}^{(q)} + \dot{\lambda}_{I,2}^{(q)}\right) \tag{22}$$

where $\dot{\lambda}_{I,1}^{(q)}$ and $\dot{\lambda}_{I,2}^{(q)}$ are the plastic multiplier rates associated with the qth line computed at the extremes of the interface, as the plastic multiplier rates vary linearly along the interfaces.

From a numerical point of view, it is worth noting that the overall constraint matrix of the optimization problem given by Eq. (20) reduced to standard form has always fewer rows than columns. For refined meshes, the ratio of columns to rows in the overall constraint matrix basically depends on the number of planes used in the linearization of the failure surface (for both the continuum and the interfaces). Furthermore, for refined meshes, the density of the overall constraint matrix is very low, and its sparsity increases as the number of elements increases. This suggests the usage of either interior-point algorithms [48,49] or the steepest edge active set algorithm [50] to solve the dual problem of Eq.(20). The steepest edge active set algorithm was found to be very efficient for the solution of the upper bound problem, but recent trends in limit analysis tend to avoid the utilization of linear pro-gramming, since the efficiency of nonlinear programming (espe-cially conic programming, see Makrodimopoulos and Martin [51] or Krabbenhoft et al. [52,53]) seems nowadays to be definitely higher. This notwithstanding, as the aim of the present paper is essentially devoted to technical applications of limit analysis to masonry structures, a consolidated interior-point algorithm is used for the sake of simplicity.

9. Effect of joint thickness on a deep beam

A structural example is analyzed in this section with the aim of showing the predictive capabilities of the proposed model as far as the bearing capacity of masonry walls is concerned. The example is a traditional benchmark for in-plane loaded brickwork, namely a masonry panel acting as a deep beam. The wall was tested by Page [54], and is 754 mm long, 457 mm high, 54 mm thick, and is supported at both sides over a length of to 188 mm, see Fig. 17. An evenly distributed load p is applied at the top of the wall through a stiff steel beam. The wall is made of half-scale pressed solid clay bricks, with dimensions $122 \times 37 \times 54$ mm^3 (length × height × depth), and 5 mm thick mortar joints.

The same test was previously numerically analyzed both by Lourenço [55] through an incremental elasto-plastic procedure, by Sutcliffe et al. [56] through a heterogeneous limit analysis approach, and by Milani et al. [23] using homogenization. In the numerical model proposed by Page [54] and by many other

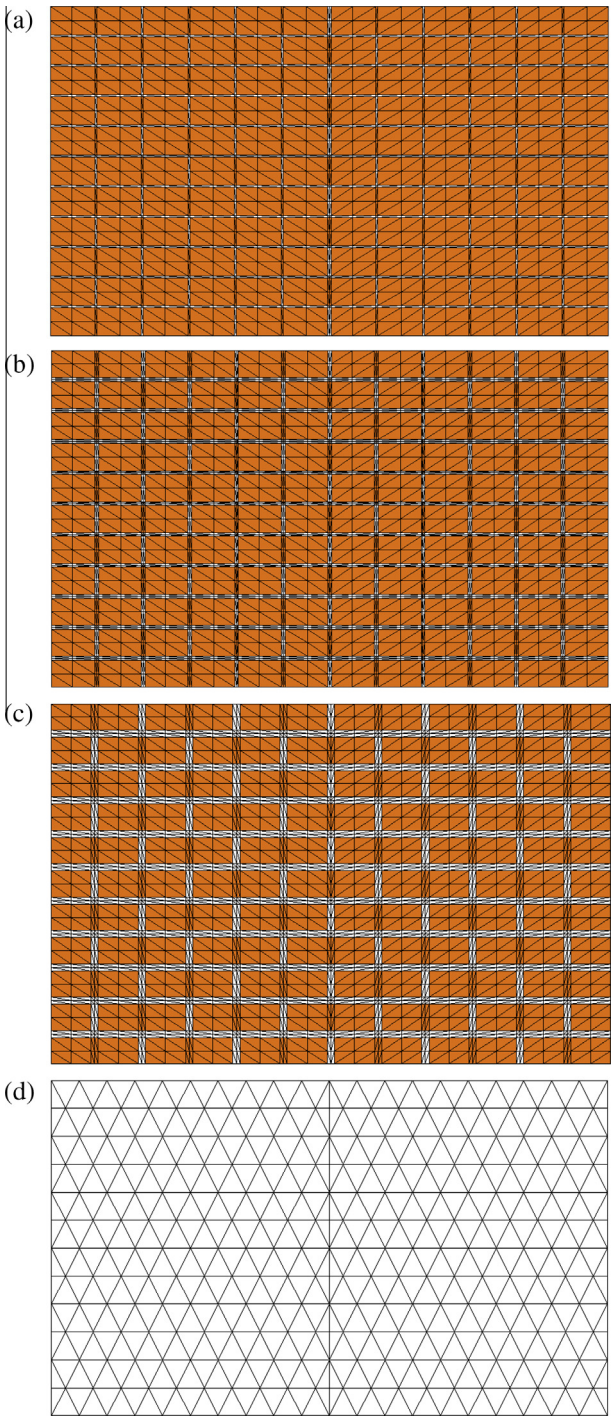

Fig. 18. FE meshes used in the analysis of a deep beam: a–c: heterogeneous models (a: joint thickness = 2.5 mm, no. of elements = 2304; b: 5 mm, 3864; c: 10 mm, 3864); d: homogenized model (no. of elements = 504).

authors, the joint thickness is neglected and units are supposed to be separated by interfaces.

To assess the effectiveness of the proposed model in predicting the bearing capacity of masonry structures with joints of different thickness, here the deep beam is assumed to have joints either of vanishing thickness, or 2.5, 5 and 10 mm thick. The accuracy of the predictions given by the homogenized model (Fig. 18d) is checked through comparisons with the results obtained with three heterogeneous FE meshes, shown in Fig. 18a–c, in addition to a mesh with units separated by interfaces. Note that the homogenized mesh is much coarser than the heterogeneous meshes.

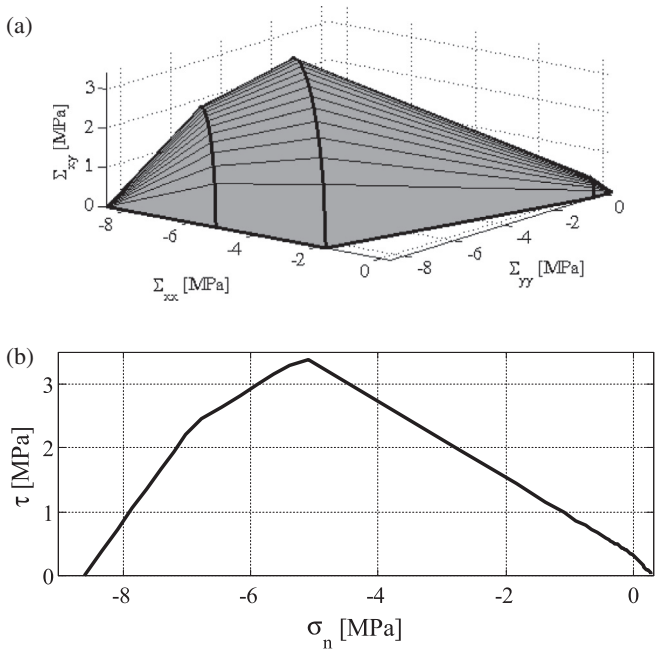

Fig. 19. Multi-linear failure surface adopted for joints. (a) Continuum (units/joints); (b) interfaces.

Table 4
Strength parameters used in the analysis of the deep beam tested by Page [54].

f_t (N/mm^2)	f_c (N/mm^2)	Φ_1	Φ_2	c (N/mm^2)
Mortar				
0.29	8.6	37°	30°	$1.4f_t$
φ				c (N/mm^2)
Units				
45°				2

In the heterogeneous models, joints and units are meshed separately, taking into account their different strength properties in the structural analysis. For mortar, a Mohr–Coulomb failure criterion with tension cutoff and multi-linear cap in compression is adopted (see Fig. 19b) with a linearization of the failure surface by means of 73 planes. For units, a Mohr–Coulomb failure criterion in plane stress is assumed (see Fig. 19a); a linearization with 48 planes of the failure surface is adopted. The strength parameters of both constituents are reported in Table 4. In the heterogeneous models, jumps in velocity are allowed within the units, within the joints, and at the interface between mortar and units; this interface is assumed to have the mechanical properties of mortar.

In the MoC-based homogenized model, the macroscopic mechanical properties are derived according to the values reported in Table 4. In Fig. 20 a few sections of the homogenized in-plane failure surfaces under biaxial tension are shown, at different orientations of the bed joint to the maximum principal stress ($\theta = 0°$, 22.5°, 45°), for joints of increasing thickness. As can be observed from the homogenized failures surfaces for $\theta = 0°$, an increase in joint thickness tends to reduce the orthotropy ratio, defined as the ratio of the horizontal to the vertical tensile strength. Accordingly, it can be expected that the reduction of joints to interfaces results into a slight overestimation of the collapse load, especially when failure is due to the formation of tension cracks for masonry working along the horizontal direction. In the applications, the homogenized failure surface is linearized at two different levels of refinement (with 24 or 160 planes). In the homogeneous model, jumps in velocity are also allowed at the interfaces between

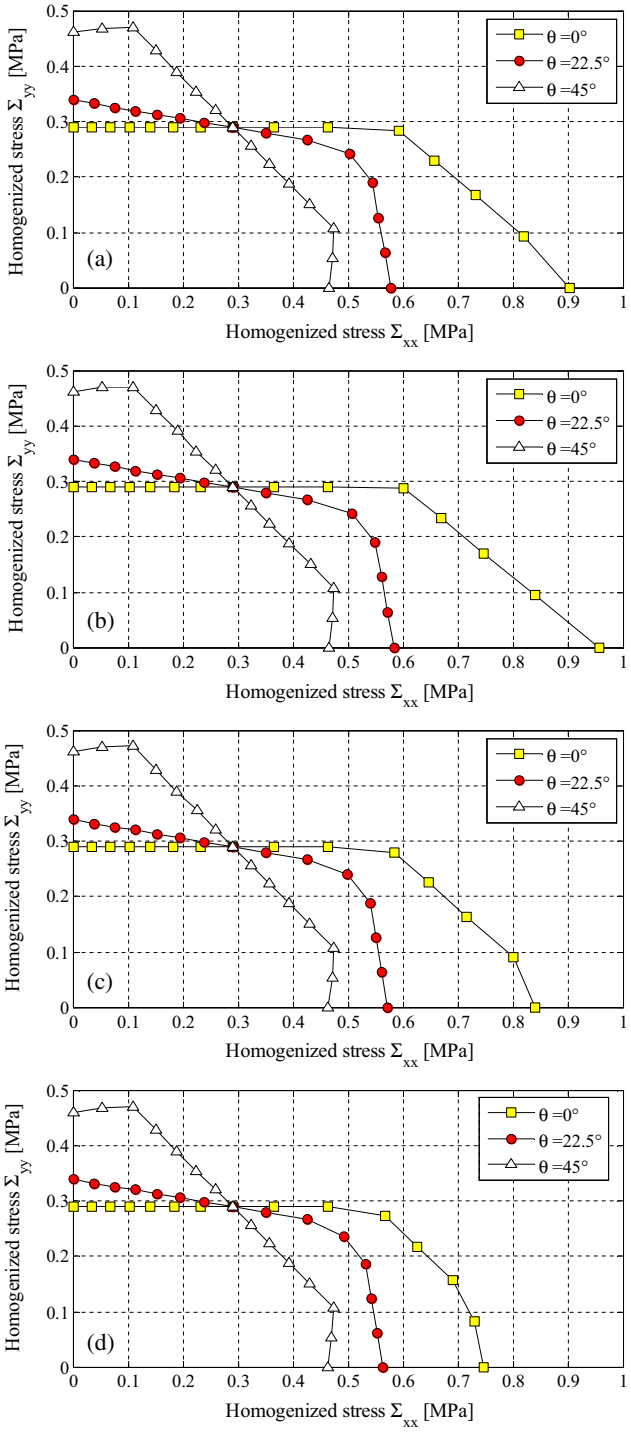

Fig. 20. Deep beam test: sections of the homogenized failure surfaces in biaxial tension at different orientations of the bed-joint to the maximum macroscopic principal stress. (a) Joint reduced to interface. (b) Joint thickness equal to 2.5 mm. (c) 5 mm. (d) 10 mm.

adjoining finite elements, consistently with the kinematics of the heterogeneous models.

Fig. 21 from a to d shows the deformed shapes at collapse for the models analyzed. In particular, Fig. 21 from a to c refers to the heterogeneous models (with joint thickness equal to 2.5, 5 and 10 mm respectively), whereas Fig. 21d shows the results of the homogenized approach. The numerical results obtained in terms of collapse load using both the discrete and the homogenized models are reported in Fig. 22.

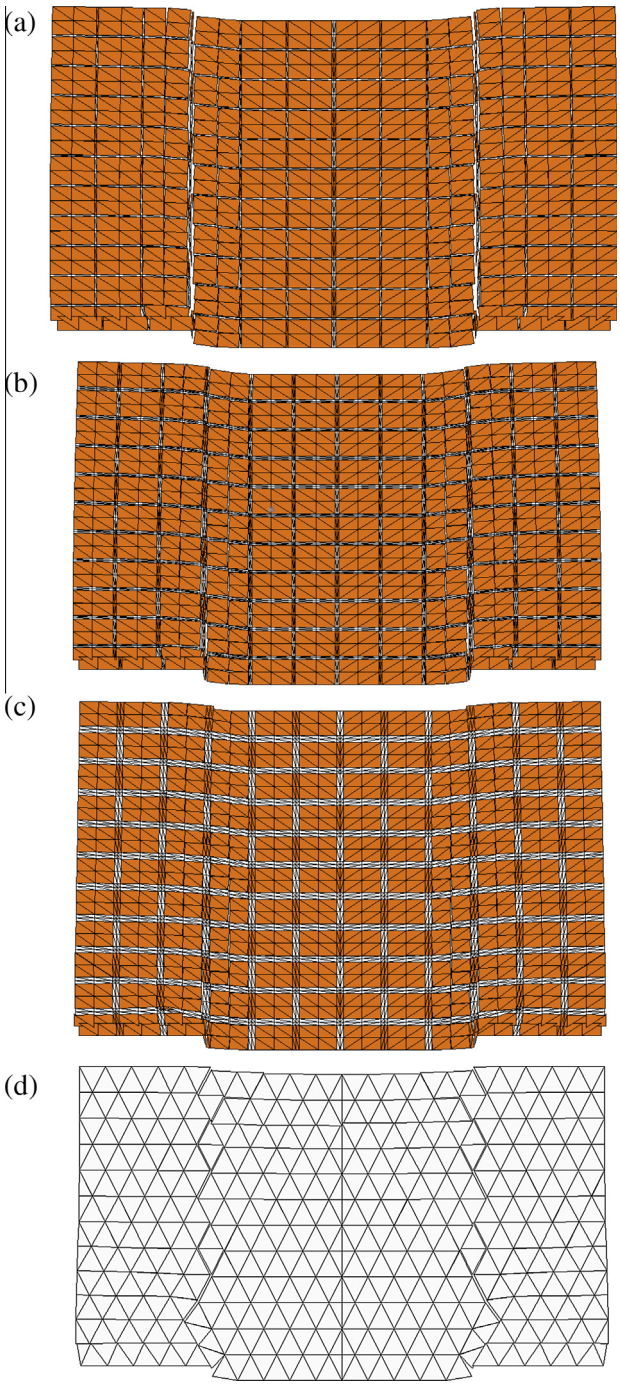

Fig. 21. Comparison among deformed shapes provided by the upper bound limit analysis FE code. From a to c, heterogeneous approach (a: joint thickness equal to 2.5 mm, b: 5 mm, c: 10 mm). d: MoC-type homogenized approach.

Both models predict a difference between the limit load computed at the two extreme values of the considered joint thickness of the order of 20%, which might be considered to fall within the engineering acceptability limits of the results, but which is not negligible in any case: this makes the reliability of models consisting of units separated by interfaces questionable. For a given thickness, the difference among the various numerical predictions is of a few percent: the most conservative estimates of the limit load are given by the homogenized approach, provided that a refined linearization of the failure surface is adopted. Finally, it is interesting to underline that the MoC-type homogenized model is capable of capturing the 'exact' collapse load predicted by the heterogeneous

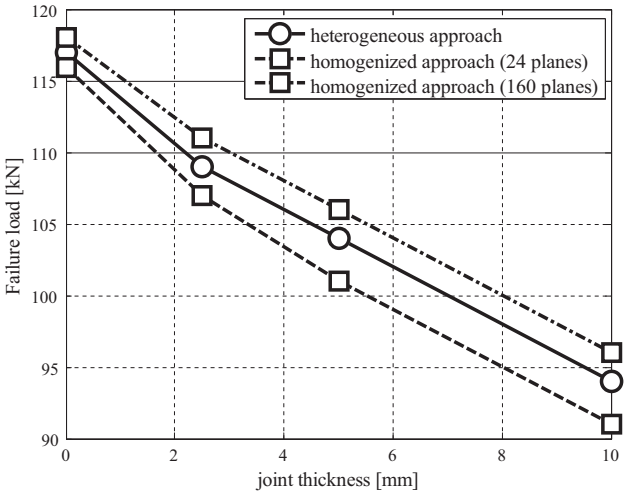

Fig. 22. Deep beam test. Failure load obtained with the heterogeneous mesh and the homogenized MoC approach at different values of the mortar joint thickness.

models for all the values of thickness inspected, even for extremely thin joints. This means that the proposed model can be adopted in engineering practice for a fast evaluation of collapse loads and failure mechanisms of real scale masonry structures, without the need of discretizing joints and units at a structural level separately.

10. Conclusions

Following an approach similar to the so-called Method of Cells, a homogenized failure criterion for periodic brickwork based on the upper bound theorem of limit analysis was derived, by formulating a piecewise differentiable strain-rate periodic velocity field over a Representative Volume Element, depending on a very limited number of degrees of freedom. The MoC-type criterion combines numerical accuracy and low computational cost. Indeed, comparisons with homogenized criteria based on the lower bound theorem of limit analysis and relying upon a refined modelling of the stress field within the RVE (Section 4) showed that the gap between the theoretical bounds is, in most cases, negligible.

Here, it is worth noting that the main points of innovation of the present approach – when compared with existing literature – are the following:

(1) The assumed discretization into rectangular sub-cells allows taking into account the actual thickness of the mortar joints and its influence in the determination of the homogenized strength domain. The majority of the models, exception made for a few attempts mainly based on the static theorem of limit analysis (see e.g. [22]), usually disregard joints thickness, adopting the concept of interface and consequently adopting for mortar a failure criterion in terms of normal and tangential stresses only. Here, a fully 2D (and hence more realistic) approach is utilized, that allows the adoption of any bi-dimensional failure criterion for the joints. Results found are in agreement with intuition and codes of practice recommendations, i.e. thick joints tend to reduce masonry strength.

(2) Conceptually, bricks and mortar are modelled in the same way, because similar rectangular sub-cells are adopted. In addition, it can be imposed that mortar and brick obey any failure criterion. As a consequence, at least in principle, it is possible to reproduce failure inside brick. Despite the well know limitations of classic limit analysis (i.e. infinite ductility, perfectly-plastic behavior of the materials and associated flow rule) and the impossibility of the model to reproduce 3D effects (particularly important for crushing in compression) as a consequence of its native 2D characterization, a satisfactory performance in reproducing experimental bi-axial tests on miniaturized panels is experienced. In particular, the approach proposed proved good ability in fitting both crack patterns and homogenized strength.

(3) When compared with alternative lower bound procedures accounting for the actual thickness of the joints, the number of inequality and equality constraints entering into the optimization problem to determine the homogenized strength is always reduced. Such numerical property allows (i) an impressive stability of the interior point algorithm and (ii) the strong reduction of the optimization time needed to achieve a converged solution, which usually required less than 5 s on PCs with standard RAM (4 Gb).

In the computation of the bearing capacity of masonry structures the use of the MoC-type homogenized criterion is particularly expedient, as finite element meshes much coarser than those needed if the heterogeneous nature of masonry is taken into account can be used, without any significant loss in accuracy (Section 9). In conclusion, it is suggested to estimate the limit load of masonry structures disregarding the presence of joints and units, and adopting the proposed macroscopic strength criterion. The case study of Section 9 showed that the 'exact' analysis of the heterogeneous structure gives a difference of only a few percent compared to that of the homogenized structure, even if the macroscopic failure surface is linearized with a limited number of planes.

In the continuation of the research, the formulation of MoC-type macroscopic strength criteria will be extended to masonry structures undergoing transverse loads. The possibility of taking more complex brick patterns (e.g. Flemish or English bond) into account will also be provided. Finally, as the brick-to-mortar interface is the weakest link in some types of masonry, especially in historic structures, failure mechanisms for the RVE defined by discontinuous velocity fields, including the possibility of dissipating power at the interfaces, will also be formulated.

Acknowledgments

The authors are grateful to Prof. Enrico Papa (University of Insubria, Italy) for providing them with experimental data of strength tests on miniaturized masonry walls.

References

[1] Portioli F, Casapulla C, Cascini L, D'Aniello M, Landolfo R. Limit analysis by linear programming of 3D masonry structures with associative friction laws and torsion interaction effects. Arch Appl Mech 2013;83:1415–38.
[2] Gilbert M, Casapulla C, Ahmed HM. Limit analysis of masonry block structures with non-associative frictional joint using linear programming. Comput Struct 2006;84:873–87.
[3] Restrepo-Vélez LF, Magenes G, Griffith MC. Dry stone masonry walls in bending-Part I: static tests. Int J Archit Heritage 2014;8(1):1–28.
[4] Lourenço PB, Rots J. A multi-surface interface model for the analysis of masonry structures. ASCE J Eng Mech 1997;123(7):660–8.
[5] Lotfi HR, Shing PB. Interface model applied to fracture of masonry structures. ASCE J Struct Eng 1994;120(1):63–80.
[6] Milani G, Zuccarello FA, Olivito RS, Tralli A. Heterogeneous upper-bound finite element limit analysis of masonry walls out-of-plane loaded. Comput Mech 2007;40(6):911–31.
[7] Milani G. 3D upper bound limit analysis of multi-leaf masonry walls. Int J Mech Sci 2008;50(4):817–36.
[8] Shieh-Beygi B, Pietruszczak S. Numerical analysis of structural masonry: mesoscale approach. Comput Struct 2008;86(21–22):1958–73.
[9] Lourenço PB, de Borst R, Rots JG. A plane stress softening plasticity model for orthotropic materials. Int J Numer Methods Eng 1997;40:4033–57.
[10] Ushaksaraei R, Pietruszczak S. Failure criterion for structural masonry based on critical plane approach. ASCE J Eng Mech 2002;128(7):769–79.

[11] Nova R, Sacchi Landriani G. A generalized failure condition for orthotropic solids. In: Boehler JP, editor. Coll int CNRS, N. 295 – Comportement mécanique des solides anisotropes; 1980. p. 623–41..
[12] Lishak VI, Yagust VI, Yankelevsky DZ. 2-D orthotropic failure criteria for masonry. Eng Struct 2012;36:360–3.
[13] Berto L, Saetta A, Scotta R, Vitaliani R. An orthotropic damage model for masonry structures. Int J Numer Methods Eng 2002;55:127–57.
[14] Pelà L, Cervera M, Roca P. Continuum damage model for orthotropic materials: application to masonry. Comput Methods Appl Mech Eng 2011; 200:917–30.
[15] Pelà L, Cervera M, Roca P. An orthotropic damage model for the analysis of masonry structures. Constr Build Mater 2013;41:957–67.
[16] Pietruszczak S, Niu X. A mathematical description of macroscopic behaviour of brick masonry. Int J Solids Struct 1992;29(5):531–46.
[17] Luciano R, Sacco E. Homogenisation technique and damage model for old masonry material. Int J Solids Struct 1997;34(24):3191–208.
[18] Luciano R, Sacco E. Damage of masonry panels reinforced by FRP sheets. Int J Solids Struct 1998;35(15):1723–41.
[19] Pegon P, Anthoine A. Numerical strategies for solving continuum damage problems with softening: application to the homogenisation of masonry. Comput Struct 1997;64(1–4):623–42.
[20] de Buhan P, de Felice G. A homogenisation approach to the ultimate strength of brick masonry. J Mech Phys Solids 1997;45(7):1085–104.
[21] Kawa M, Pietruszczak S, Shieh-Beygi B. Limit states for brick masonry based on homogenization approach. Int J Solids Struct 2008;45:998–1016.
[22] Milani G, Lourenço PB, Tralli A. Homogenised limit analysis of masonry walls. Part I: failure surfaces. Comput Struct 2006;84(3–4):166–80.
[23] Milani G, Lourenço PB, Tralli A. Homogenised limit analysis of masonry walls. Part II: structural examples. Comput Struct 2006;84(3–4):181–95.
[24] Milani G. Simple homogenization model for the non-linear analysis of in-plane loaded masonry walls. Comput Struct 2011;89(17–18):1586–601.
[25] Milani G, Lourenço PB, Tralli A. Homogenization approach for the limit analysis of out-of-plane loaded masonry walls. ASCE J Struct Eng 2006;132(10): 1650–63.
[26] Cecchi A, Milani G, Tralli A. A Reissner–Mindlin limit analysis model for out-of-plane loaded running bond masonry walls. Int J Solids Struct 2007;44(5): 1438–60.
[27] Milani G. Simple lower bound limit analysis homogenization model for in- and out-of-plane loaded masonry wall. Constr Build Mater 2011;25:4426–43.
[28] Cecchi A, Milani G. A kinematic FE limit analysis model for thick English bond masonry walls. Int J Solids Struct 2008;45(5):1302–31.
[29] Milani G. Homogenized limit analysis of FRP-reinforced masonry walls out-of-plane loaded. Comput Mech 2009;43:617–39.
[30] Milani G. Kinematic FE limit analysis homogenization model for masonry walls reinforced with continuous FRP grids. Int J Solids Struct 2011;48(2): 326–45.
[31] Suquet P. Analyse limite et homogénéisation. C R Acad Sci – Sér IIB Méc 1983;296:1355–8.
[32] Aboudi J. Mechanics of composite materials: a unified micromechanical approach, Studies in Applied Mechanics, vol. 29. Amsterdam: Elsevier; 1991.
[33] Taliercio A. Closed-form expressions for the macroscopic in-plane elastic and creep coefficients of brick masonry. Int J Solids Struct 2014;51(17):2949–63.
[34] Ganz HR. Masonry walls subjected to normal and shear forces (in German). Ph.D. thesis. Zurich (Switzerland): Institute of Structural Engineering, ETH Zurich; 1985..
[35] Mojsilović N. Strength of masonry subjected to in-plane loading: a contribution. Int J Solids Struct 2011;48(6):865–73.
[36] Papa E, Nappi A. A numerical approach for the analysis of masonry structures. Masonry Int 1993;7:18–24.
[37] Salençon J. Calcul à la rupture et analyse limite. Paris: Presses de l'École nationale des Ponts et Chaussées; 1992.
[38] Fletcher R. Practical methods of optimization. 2nd ed. New York: Wiley; 2000.
[39] Mojsilovic N, Stewart MG. Probability and structural reliability assessment of mortar joint thickness in load-bearing masonry walls. Struct Safety 2015;52: 209–18.
[40] Hilsdorf HK. Investigation into the failure mechanism of brick masonry loaded in axial compression. In: Proc int conf on masonry structural systems, Houston, Texas; 1969. p. 34–41..
[41] Francis AJ, Horman CB, Jerrems LE. The effects of joint thickness and other factors on the compressive strength of brickwork. In: Proceedings of the second international brick masonry conference. British Masonry Society, Stoke-on-Trent; 1981. p. 31–7..
[42] Anthoine A. Homogenization of periodic masonry: plane stress, generalized plane strain or 3D modelling?. Commun Numer Methods Eng 1997;13(5): 319–26.
[43] Addessi D, Sacco E. A kinematic enriched plane state formulation for the analysis of masonry panels. Eur J Mech A/Solids 2014;44:188–200.
[44] Colliat JB, Davenne L, Ibrahimbegovic A. Modélisation jusqu'à rupture de murs en maçonnerie chargés dans leur plan. Rev Française Génie Civ 2002;4: 593–606.
[45] Ibrahimbegovic A, Colliat JB, Davenne L. Thermomechanical coupling in folded plates and non-smooth shells. Comput Methods Appl Mech Eng 2005;194: 2686–707.
[46] Page AW. The biaxial compressive strength of brick masonry. Proc Instn Civ Eng, Part 1981;2(71):893–906.
[47] Sloan SW, Kleeman PW. Upper bound limit analysis using discontinuous velocity fields. Comput Methods Appl Mech Eng 1995;127(1–4):293–314.
[48] Mehrotra S. On the implementation of a (primal-dual) interior point method. SIAM J Optim 1992;2(4):575–601.
[49] Karmarkar N. A new polynomial-time algorithm for linear programming. Combinatorics 1984;4:373–95.
[50] Sloan SW. Lower bound limit analysis using finite elements and linear programming. Int J Numer Anal Methods Geomech 1988;12:61–77.
[51] Makrodimopoulos A, Martin CM. Lower bound limit analysis of cohesive-frictional materials using second-order cone programming. Int J Numer Methods Eng 2006;66(4):604–34.
[52] Krabbenhoft K, Lyamin AV, Sloan SW. Formulation and solution of some plasticity problems as conic programs. Int J Solids Struct 2007;44: 1533–49.
[53] Krabbenhoft K, Lyamin AV, Sloan SW. Three-dimensional Mohr–Coulomb plasticity using semidefinite programming. Commun Numer Methods Eng 2008;24:1107–19.
[54] Page AW. Finite element model for masonry. ASCE J Struct Div 1978;104(8): 1267–85.
[55] Lourenço PB. Computational strategies for masonry structures. PhD thesis. The Netherlands: TU Delft; 1996..
[56] Sutcliffe DJ, Yu HS, Page AW. Lower bound limit analysis of unreinforced masonry shear walls. Comput Struct 2001;79:1295–312.